9-1-2003

Corrugated Web Girder Shape and Strength Criteria

Richard Sause

Hassam H. Abbas

Wagdy G. Wassef

Robert G. Driver

Mohamed Elgaaly

Corrugated Web Girder Shape and Strength Criteria

Work Area 1
Pennsylvania Innovative High Performance Steel
Bridge Demonstration Project

Report to
Commonwealth of Pennsylvania
Department of Transportation
Contract No. 359810

by

Richard Sause, Hassan H. Abbas, Wagdy G. Wassef,
Robert G. Driver, and Mohamed Elgaaly

ATLSS Report No. 03-18

September 2003

ATLSS is a National Center for Engineering Research
on Advanced Technology for Large Structural Systems

117 ATLSS Drive
Bethlehem, PA 18015-4729

Phone: (610)758-3525
Fax: (610)758-5902

www.atlss.lehigh.edu
Email: inatl@lehigh.edu

Technical Report Documentation Page

1. Report No.	2. Government Accession No.	3. Recipient's Catalog No.
FHWA-PA-2004-005-98-10 (a)		

4. Title and Subtitle	5. Report Date
Corrugated Web Girder Shape and Strength Criteria: Work Area 1, Pennsylvania Innovative High Performance Steel Bridge Demonstration Project	September 2003
	6. Performing Organization Code 4D371 (CAGE)
7. Author(s) Richard Sause, Hassan H. Abbas, Wagdy G. Wassef, Robert G. Driver, and Mohamed Elgaaly	**8. Performing Organization Report No.** ATLSS Report No. 03-18
9. Performing Organization Name and Address Advanced Technology for Large Structural Systems (ATLSS) Center Lehigh University 117 ATLSS Drive Bethlehem PA 18015-4729	**10. Work Unit No. (TRAIS)**
	11. Contract or Grant No. 359810
12. Sponsoring Agency Name and Address The Pennsylvania Department of Transportation Bureau of Planning and Research Commonwealth Keystone Building 400 North Street, 6th Floor Harrisburg, PA 17120-0064	**13. Type of Report and Period Covered** Final Report
	14. Sponsoring Agency Code

15. Supplementary Notes
COTR: Thomas P. Macioce

See Report Nos.: FHWA-PA-2004-005-98-10 (b), (c), (d), and (e) for related work.

16. Abstract
The Pennsylvania Department of Transportation (PennDOT) has proposed to design and construct a high performance steel demonstration bridge using HPS-485W (HPS-70W) steel in combination with I-shaped girders with corrugated webs. Toward this goal, a coordinated program of design and fabrication studies, and applied laboratory research (testing and analysis) has been conducted to develop details and design criteria for the bridge. This program, titled the "Pennsylvania High Performance Steel Bridge Demonstration Project", consisted of the following Work Areas: (1) corrugated web girder corrugation shape and strength criteria; (2) corrugated web girder fabrication; (3) fatigue resistance of corrugated web girders; (4) corrugated web girder field splices; and (5) diaphragms with flange rotational restraint braces. This report addresses Work Area 1, corrugated web girder corrugation shape and strength criteria.

The report describes work conducted to establish design criteria for the shear and flexural strength of corrugated web girders, and to recommend a corrugation shape for the girders of the demonstration bridge. The report summarizes prior shear strength theory and test results for corrugated web girders. New shear strength criteria are developed, and the results from new large-scale shear strength tests of HPS-485W (HPS-70W) steel corrugated web girders are presented. Flexural strength theory and test results are reviewed and new flexural theory for corrugated web girders is presented. A preliminary design study that was used to select the corrugation shape for the demonstration bridge is presented. Finally, shear and flexural strength design criteria are recommended.

17. Key Words	18. Distribution Statement
Steel bridge, steel bridge girder, steel girder strength, shear strength, flexural strength, corrugated web, corrugated web girder, corrugated web girder stability, corrugated web girder strength, high performance steel	No restrictions. This document is available from the National Technical Information Service, Springfield, VA 22161 or by request to the PennDOT Research Program.

19. Security Classif. (of this report)	20. Security Classif. (of this page)	21. No. of Pages	22. Price
Unclassified	Unclassified	52	

Form DOT F 1700.7 **(8-72)** **Reproduction of completed page authorized**

Corrugated Web Girder Shape and Strength Criteria

Work Area 1
Pennsylvania Innovative High Performance Steel
Bridge Demonstration Project

Report to
Commonwealth of Pennsylvania
Department of Transportation
Contract No. 359810

by

Richard Sause, Ph.D.
Professor of Structural Engineering
Lehigh University

Hassan H. Abbas, Ph.D.
Formerly, Graduate Research Assistant
Lehigh University

Wagdy G. Wassef, Ph.D.
Associate
Modjeski and Masters, Inc.

Robert G. Driver, Ph.D.
Associate Professor of Civil Engineering
University of Alberta

Mohamed Elgaaly, Ph.D.
Professor of Civil Engineering
Drexel University

ATLSS Report No. 03-18

September 2003

ATLSS is a National Center for Engineering Research
on Advanced Technology for Large Structural Systems

117 ATLSS Drive
Bethlehem, PA 18015-4729

Phone: (610)758-3525
Fax: (610)758-5902

www.atlss.lehigh.edu
Email: inatl@lehigh.edu

Acknowledgements

This work was sponsored by the Pennsylvania Department of Transportation. Support was also provided by the Federal Highway Administration and the Pennsylvania Infrastructure Technology Alliance (funded by a grant from Pennsylvania Department of Community and Economic Development).

The Pennsylvania High Performance Steel Bridge Demonstration Project is a partnership of the ATLSS Center at Lehigh University with Drexel University (M. Elgaaly), High Steel Structures, Inc. (S. Kopp, R. Kase), and Modjeski and Masters, Inc. (W. Wassef), and involves many individuals (the primary contacts are given in parentheses). This report addresses Work Area 1 of this project. The contributions of S. Kopp and R. Kase of High Steel Structures, Inc. to the planning stages of Work Area 1 are acknowledged. The corrugated web girder test specimens used in Work Area 1 were fabricated by High Steel Structures, Inc. The authors are grateful for the input and support of Tom Macioce, Bob Horwhat, Dave Wilhelm, and Joe Bracken from the Pennsylvania Department of Transportation. Finally, the authors are grateful for the contributions of D. Yu and T. Clarke, and the contributions of the technical staff of the ATLSS Center and Fritz Engineering Lab.

Table of Contents

Section		Page
1.	Introduction	1
2.	Shear Strength of Corrugated Web Girders	2
2.1.	Theoretical Shear Strength	2
2.2.	Comparison of Theoretical Shear Strength with Existing Test Data	5
2.3.	Proposed Nominal Shear Strength Equation	10
3.	Shear Strength Tests of Corrugated Web Girders	12
3.1.	Design and Fabrication of Test Specimens	13
3.2.	Finite Element Analyses of Test Specimens	14
3.3.	Measurement of Specimen Imperfections and Preliminary Tests	17
3.4.	Set-up and Instrumentation for Shear Strength Tests	21
3.5.	Results and Observations from Shear Strength Tests	23
3.6.	Analysis and Discussion of Results from Shear Strength Tests	25
4.	Flexural Strength of Corrugated Web Girders	27
4.1.	Flexural Strength	27
4.2.	Strength under Combined Flexure and Shear	29
5.	Preliminary Design Study of Corrugated Web Bridge Girders	36
5.1.	Design Parameters	37
5.2.	Flat Web I-Girders	37
5.3.	Corrugated Web Girders with Trapezoidal Corrugations	38
5.4.	Corrugated Web Girders with Sinusoidal Corrugations	45
5.5.	Observations from Preliminary Design Study	50
6.	Strength Design Criteria for Corrugated Web Girders	51
6.1.	Design Criteria for Shear Resistance	51
6.2.	Design Criteria for Flexural Resistance	53
7.	Recommended Corrugation Geometry	58
8.	Summary and Conclusions	60
References		61

List of Tables

Table		Page
Table 1.	US tests (Elgaaly *et al.* 1996)	6
Table 2.	European tests (Lindner and Aschinger 1988; Peil 1998)	8
Table 3.	Flat web I-girder dimensions	38
Table 4.	Flange dimensions for corrugated web girders	40
Table 5.	Web thickness of trapezoidal web girders and weight comparison to flat web I-girders - no web thickness limit	42
Table 6.	Weight comparison of trapezoidal web girders to flat web I-girders – 6mm minimum web thickness	43
Table 7.	Weight comparison of trapezoidal web girders to flat web I-girders – 9mm minimum web thickness	44
Table 8.	Web thickness of sinusoidal web girders and weight comparison to flat web I-girders - no web thickness limit	47
Table 9.	Weight comparison of sinusoidal web girders to flat web I-girders – 6mm minimum web thickness	48
Table 10.	Weight comparison of sinusoidal web girders to flat web I-girders – 9mm minimum web thickness	49

List of Figures

Figure		Page
Figure 1.	Trapezoidal corrugated web	2
Figure 2.	Variation of $F(\alpha, \beta)$ with corrugation geometry	4
Figure 3.	Comparison of calculated shear strength with test results	10
Figure 4.	Comparison of shear strength from Equation 7 with test results	11
Figure 5.	Corrugated web shear test specimens (dimensions in mm)	12
Figure 6.	Shear buckling modes from FE analysis of shear test specimens	14
Figure 7.	Shear buckling coefficients from FE analysis of shear test specimens	15
Figure 8.	Shear stress capacity from FE analysis versus imperfection amplitude	16
Figure 9.	Shear stress capacity from FE analysis versus imperfection shape	17
Figure 10.	Schematic of web initial out-of-flatness geometric imperfections	17
Figure 11.	Measured web geometric imperfections for Girders G7A and G8A	18
Figure 12.	Web fold deflection measurement rig	19
Figure 13.	Manual and automated measurements of web geometric imperfections	20
Figure 14.	Web out-of-plane deflections under loading for Fold 8 of Girder G7A	21
Figure 15.	Test specimen in five million pound universal testing machine	21
Figure 16.	Lateral brace arrangement	22
Figure 17.	Load versus deflection for Girder G7A	23
Figure 18.	Load versus deflection for Girder G8A	23
Figure 19.	Girder G7A after failure	24
Figure 20.	Girder G8A after failure	25

List of Figures (continued)

Figure		Page
Figure 21.	Longitudinal strains over girder depth at Fold 8 of Girder G7A	26
Figure 22.	Free body diagrams of corrugated web I-girder components	30
Figure 23.	Fictitious load patterns	32
Figure 24.	Flange transverse bending for even number of half corrugations	33
Figure 25.	Flange transverse bending for odd number of half corrugations	34
Figure 26.	Corrugation geometries (dimensions in mm)	39
Figure 27.	Sinusoidal and corresponding trapezoidal corrugation geometry	45

Abstract

The Pennsylvania Department of Transportation (PennDOT) has proposed to design and construct a high performance steel demonstration bridge using HPS-485W (HPS-70W) steel in combination with I-shaped girders with corrugated webs. To assist PennDOT, a coordinated program of design and fabrication studies, and applied laboratory research (testing and analysis) has been conducted to develop details and design criteria for the bridge. This project, titled the "Pennsylvania High Performance Steel Bridge Demonstration Project", is being conducted by the following team: (1) the ATLSS Center at Lehigh University, (2) Modjeski and Masters, Inc., (3) High Steel Structures, Inc., and (4) Drexel University. The program consists of the following Work Areas: (1) corrugated web girder corrugation shape and strength criteria; (2) corrugated web girder fabrication; (3) fatigue resistance of corrugated web girders; (4) corrugated web girder field splices; and (5) precast deck and diaphragms with flange rotational restraint braces. This report addresses Work Area 1, corrugated web girder corrugation shape and strength criteria.

The report describes work conducted to establish design criteria for the shear and flexural strength of corrugated web girders, and to recommend a corrugation shape for the girders of the demonstration bridge. The report summarizes prior shear strength theory and test results for corrugated web girders. New shear strength criteria are developed, and the results from new large-scale shear strength tests of HPS-485W (HPS-70W) steel corrugated web girders are presented. Flexural strength theory and test results are reviewed and new flexural theory for corrugated web girders is presented. A preliminary design study that was used to select the corrugation shape for the demonstration bridge is presented. Finally, shear and flexural strength design criteria are recommended.

1. Introduction

The Pennsylvania Department of Transportation (PennDOT) has proposed to design and construct a HPS demonstration bridge using HPS-485W (HPS-70W) steel in combination with innovative bridge design concepts. The site of the bridge is to be determined. The demonstration bridge will be a multiple steel I-girder bridge. The girders will be fabricated with corrugated webs, and may be braced with cross-frames that include compression flange rotational restraint braces. Precast high-performance concrete panels may be used to construct the deck without extensive use of field-placed concrete. To assist PennDOT with the development of the demonstration bridge, a coordinated program of design and fabrication studies, and applied laboratory research (testing and analysis) has been conducted to develop details and design criteria for the bridge. This project, titled the "Pennsylvania High Performance Steel (HPS) Bridge Demonstration Project", is being conducted by a team composed of the following participants: (1) the ATLSS Center at Lehigh University, (2) Modjeski and Masters, Inc., (3) High Steel Structures, Inc., and (4) Drexel University.

The coordinated program of design and fabrication studies, and applied laboratory research (testing and analysis) consists of the following work areas: (1) corrugated web girder corrugation shape and strength criteria; (2) corrugated web girder fabrication; (3) fatigue resistance of corrugated web girders; (4) corrugated web girder field splices; and (5) precast deck and diaphragms with flange rotational restraint braces. This report addresses only Work Area 1, corrugated web girder corrugation shape and strength criteria.

The objectives of this report are: (1) to establish design criteria for the shear and flexural strength of corrugated web girders, and (2) to recommend a corrugation shape for the girders of the demonstration bridge. To accomplish these objectives, previous shear strength theory and test results for corrugated web girders are summarized and analyzed. New shear strength criteria are developed, and the results from new large-scale shear strength tests of ASTM A709, grade HPS-485W (HPS-70W) steel (ASTM 2001)corrugated web girders are presented. Flexural strength theory and test results are reviewed and new flexural strength theory is presented. The results of a preliminary design study that was used to select the corrugation shape for the demonstration bridge are presented. Shear strength and flexural strength design criteria are presented, and a corrugation shape for the demonstration bridge is recommended.

Section 2 of the report begins with a summary and analysis of shear strength theory and test results from the literature. Based on the theory and test results, a formula for the nominal shear strength of corrugated web bridge girders is proposed at the end of Section 2. Section 3 summarizes the results of shear strength tests conducted as part of Work Area 1. The results are used to verify the nominal shear strength criteria. Flexural strength is then discussed in Section 4. Section 5 presents a design study of corrugated web bridge girders. Section 6 summarizes the recommended shear and flexural strength design criteria. Section 7 recommends the corrugation profile for the demonstration bridge, and Section 8 summarizes the report and provides conclusions.

2. Shear Strength of Corrugated Web Girders

The shear strength of corrugated web girders is a function of the web depth, thickness, corrugation geometry, and materials. The corrugations provide stability to the web, eliminating the need for transverse stiffeners. Thus, the shear strength does not depend on the presence or spacing of transverse stiffeners. Corrugated webs do not carry significant longitudinal stresses from overall (primary) bending of the girders, and the bending moment is assumed to be carried entirely by the flanges. This section discusses the shear strength of corrugated web girders. First, the shear strength based on theory is presented. Then the theoretical shear strength is compared with test results found in the literature. The comparison shows the theoretical shear strength equations are not accurate, and a new shear strength formula is proposed.

2.1. Theoretical Shear Strength

Corrugated webs have been found to fail by shear buckling. Both local and global buckling modes have been observed experimentally. In theory, local buckling involves a single fold. Global buckling involves multiple folds, with buckles extending over the entire depth of the web. In this section, theoretical equations for the shear buckling strength of corrugated webs are presented for webs with a trapezoidal corrugation shape (see Figure 1 for notation).

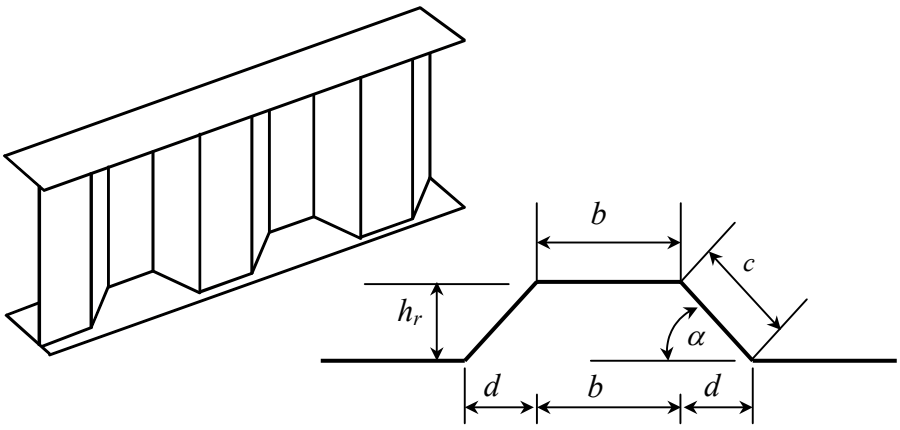

Figure 1. Trapezoidal corrugated web.

Local buckling has been predicted using classical plate buckling theory (*e.g.*, Timoshenko and Gere 1961), in which a given fold (longitudinal or inclined) is assumed to be supported by adjacent folds along its vertical edges and by the flanges along its horizontal edges. The elastic shear buckling stress is given by:

$$(\tau_{cr,L})_{el} = k_L \frac{\pi^2 E}{12(1-\nu^2)(w/t_w)^2} \tag{1}$$

where E and ν are the elastic modulus and Poisson's ratio, respectively, w is the maximum fold width (maximum of the longitudinal fold width, b, and the inclined fold width, c, shown in Figure 1), t_w is the web thickness, and k_L is a factor that depends upon the boundary conditions and the fold aspect ratio. A small aspect ratio, w/h_w (where h_w is the web depth), minimizes k_L, and in this case, k_L lies between 5.34 (assuming the fold has simply supported edges) and 8.98 (assuming the fold has fixed edges).

Global buckling has been predicted by treating the corrugated web as an orthotropic flat web for which the elastic shear buckling stress is (Easley 1975):

$$(\tau_{cr,G})_{el} = k_G \frac{D_x^{1/4} D_y^{3/4}}{t_w h_w^2} \tag{2}$$

where D_x and D_y are the orthotropic plate stiffnesses about the weak and strong axis, respectively, and k_G is a factor that depends upon the boundary conditions. For an infinitely long web (which minimizes k_G), the bounding values for k_G (Elgaaly *et al.* 1996) are 31.6 (assuming the web is simply supported by the flanges) and 59 (assuming the flanges provide the web with fixed supports).

Upon substituting expressions for D_x and D_y, it is possible to rewrite Equation 2 in the following form:

$$(\tau_{cr,G})_{el} = k_G \frac{E\, t_w^{1/2}\, b^{3/2}}{12\, h_w^2} F(\alpha, \beta) \tag{3}$$

where $F(\alpha, \beta)$ is a nondimensional coefficient characterizing the web corrugation geometry that is given by:

$$F(\alpha, \beta) = \sqrt{\frac{(1+\beta)\sin^3 \alpha}{\beta + \cos\alpha}} \cdot \left\{ \frac{3\beta + 1}{\beta^2 (\beta + 1)} \right\}^{3/4} \tag{4}$$

where α is the corrugation angle (see Figure 1), and β is the ratio of the longitudinal fold width, b, to the inclined fold width, c. Figure 2 demonstrates that the global buckling capacity (as reflected by the coefficient $F(\alpha, \beta)$) increases with decreasing β and increasing α for a constant t_w, b, and h_w. However, small values of β will result in inefficient use of the web plate material and should be avoided. β values between 1 and 2, and α values between 30 and 45 degrees are often used.

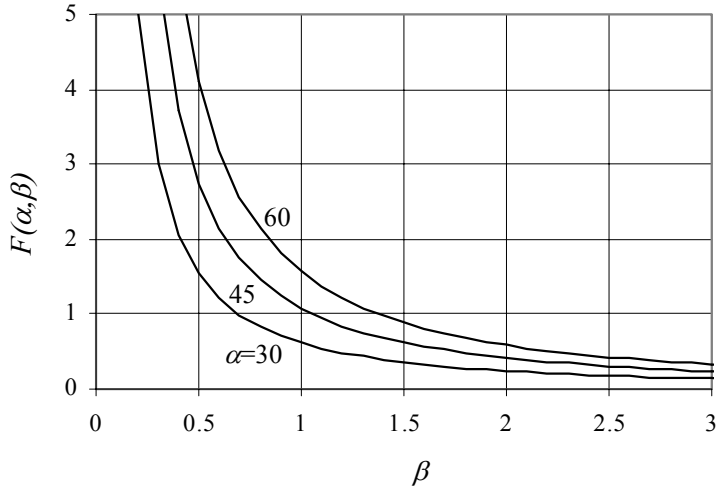

Figure 2. Variation of $F(\alpha, \beta)$ with corrugation geometry.

When the elastic shear buckling stress exceeds 80% of the shear yield stress, τ_y, the following inelastic buckling stress equation (Elgaaly *et al.* 1996) is used for both local buckling ($(\tau_{cr})_{el}$ from Equation 1) and global buckling ($(\tau_{cr})_{el}$ from Equation 3):

$$(\tau_{cr})_{inel} = \sqrt{0.8\,\tau_y\,(\tau_{cr})_{el}} \le \tau_y \tag{5}$$

where τ_y is given by the von Mises yield criterion:

$$\tau_y = \frac{F_y}{\sqrt{3}} \tag{6}$$

with F_y equal to the uniaxial yield stress of the web material.

The theory is summarized as follows. Two corrugated web shear buckling modes are identified: local buckling of a fold, and global buckling of the web. The elastic buckling stress is given by Equation 1 for the local buckling mode and Equation 3 for the global buckling mode. When the elastic shear buckling stress exceeds 80% of the shear yield stress, τ_y, the inelastic buckling stress is given by Equation 5. Equation 5 applies to both the local and global buckling modes.

2.2. Comparison of Theoretical Shear Strength with Existing Test Data

Many shear strength tests of corrugated web beams with trapezoidal web profiles have been conducted worldwide. In the US, Elgaaly *et al.* (1996) reported the results of 42 tests on 21 beams. In Europe, Lindner and Aschinger (1988) summarized the results of 25 tests from Germany, Sweden, and Finland. Peil (1998) reported the results of 20 tests on relatively large size girders.

Tests conducted in the US (Elgaaly *et al.* 1996) and in Europe (Lindner and Aschinger 1988; Peil 1998) are summarized in Tables 1 and 2, respectively. The following notation is used in the tables:

a is the shear span length,
V_e is the maximum experimental shear force,
τ_e is the maximum experimental nominal shear stress, equal to $V_e/(h_w t_w)$,
$\tau_{cr,L}$ is the local buckling stress from Equations 1 or 5,
$\tau_{cr,G}$ is the global buckling stress from Equations 3 or 5,
τ_{cr} is the minimum of $\tau_{cr,L}$ and $\tau_{cr,G}$,
τ_n is the nominal shear strength from Equation 7 (see page 11).

In calculating $\tau_{cr,L}$ and $\tau_{cr,G}$, simply-supported boundary conditions were assumed to provide lower bound results, and, therefore, k_L equal to 5.34 and k_G equal to 31.6 were used. The ratio τ_e/τ_{cr}, given in column 20 of Tables 1 and 2, is used as a means of assessing the theoretical shear buckling stress equations. The average ratio of τ_e/τ_{cr} for all the tests is approximately 1.06. However, a close examination of column 20 of Tables 1 and 2 shows that a large number of tests give ratios of τ_e/τ_{cr} that are substantially less than 1, indicating that the theoretical buckling stress equations, while reasonable in the average sense, may overestimate the shear strength in some cases.

Table 1. US tests (Elgaaly *et al.* 1996).

ID	Specimen	a	h_w	t_w	b	d	h_r	α	β	w/t_w	$F(\alpha,\beta)$
(1)	(2)	(mm) (3)	(mm) (4)	(mm) (5)	(mm) (6)	(mm) (7)	(mm) (8)	(deg.) (9)	(10)	(11)	(12)
1	V-PILOTA	304.8	304.8	0.7823	38.1	25.4	25.4	45	1.06	49	1.00
2	V-PILOTB	304.8	304.8	0.7849	38.1	25.4	25.4	45	1.06	49	1.00
3	V121216A	304.8	304.8	0.6375	38.1	25.4	25.4	45	1.06	60	1.00
4	V121216B	304.8	304.8	0.7645	38.1	25.4	25.4	45	1.06	50	1.00
5	V181216B	304.8	457.2	0.6096	38.1	25.4	25.4	45	1.06	63	1.00
6	V181216C	304.8	457.2	0.7595	38.1	25.4	25.4	45	1.06	50	1.00
7	V181816A	457.2	457.2	0.6350	38.1	25.4	25.4	45	1.06	60	1.00
8	V181816B	457.2	457.2	0.7366	38.1	25.4	25.4	45	1.06	52	1.00
9	V241216A	304.8	609.6	0.6350	38.1	25.4	25.4	45	1.06	60	1.00
10	V241216B	304.8	609.6	0.7874	38.1	25.4	25.4	45	1.06	48	1.00
11	V121221A	304.8	304.8	0.6299	41.91	23.4	33.3	55	1.03	67	1.35
12	V121221B	304.8	304.8	0.7849	41.91	23.4	33.3	55	1.03	53	1.35
13	V122421A	609.6	304.8	0.6756	41.91	23.4	33.3	55	1.03	62	1.35
14	V122421B	609.6	304.8	0.7823	41.91	23.4	33.3	55	1.03	54	1.35
15	V181221A	304.8	457.2	0.6096	41.91	23.4	33.3	55	1.03	69	1.35
16	V181221B	304.8	457.2	0.7620	41.91	23.4	33.3	55	1.03	55	1.35
17	V181821A	457.2	457.2	0.6350	41.91	23.4	33.3	55	1.03	66	1.35
18	V181821B	457.2	457.2	0.7366	41.91	23.4	33.3	55	1.03	57	1.35
19	V241221A	304.8	609.6	0.6096	41.91	23.4	33.3	55	1.03	69	1.35
20	V241221B	304.8	609.6	0.7620	41.91	23.4	33.3	55	1.03	55	1.35
21	V121232A	304.8	304.8	0.6401	49.784	26.4	50.8	62.5	0.87	89	2.00
22	V121232B	304.8	304.8	0.7798	49.784	26.4	50.8	62.5	0.87	73	2.00
23	V121832A	457.2	304.8	0.6401	49.784	26.4	50.8	62.5	0.87	89	2.00
24	V121832B	457.2	304.8	0.9195	49.784	26.4	50.8	62.5	0.87	62	2.00
25	V122432A	609.6	304.8	0.6401	49.784	26.4	50.8	62.5	0.87	89	2.00
26	V122432B	609.6	304.8	0.7772	49.784	26.4	50.8	62.5	0.87	74	2.00
27	V181232A	304.8	457.2	0.5969	49.784	26.4	50.8	62.5	0.87	96	2.00
28	V181232B	304.8	457.2	0.7493	49.784	26.4	50.8	62.5	0.87	76	2.00
29	V181832A	457.2	457.2	0.6096	49.784	26.4	50.8	62.5	0.87	94	2.00
30	V181832B	457.2	457.2	0.7493	49.784	26.4	50.8	62.5	0.87	76	2.00
31	V241232A	304.8	609.6	0.6223	49.784	26.4	50.8	62.5	0.87	92	2.00
32	V241232B	304.8	609.6	0.7620	49.784	26.4	50.8	62.5	0.87	75	2.00
33	V121809A	457.2	304.8	0.7061	19.812	11.9	14.2	50	1.07	28	1.14
34	V121809C	457.2	304.8	0.6325	19.812	11.9	14.2	50	1.07	31	1.14
35	V122409A	609.6	304.8	0.7137	19.812	11.9	14.2	50	1.07	28	1.14
36	V122409C	609.6	304.8	0.6629	19.812	11.9	14.2	50	1.07	30	1.14
37	V181209A	304.8	457.2	0.5588	19.812	11.9	14.2	50	1.07	35	1.14
38	V181209C	304.8	457.2	0.6096	19.812	11.9	14.2	50	1.07	33	1.14
39	V181809A	457.2	457.2	0.6096	19.812	11.9	14.2	50	1.07	33	1.14
40	V181809C	457.2	457.2	0.6223	19.812	11.9	14.2	50	1.07	32	1.14
41	V241209A	304.8	609.6	0.6223	19.812	11.9	14.2	50	1.07	32	1.14
42	V241209C	304.8	609.6	0.6350	19.812	11.9	14.2	50	1.07	31	1.14

Table 1. US tests (Elgaaly *et al.* 1996) (continued).

ID (13)	V_e (kN) (14)	F_y (MPa) (15)	τ_y (MPa) (16)	τ_e/τ_y (17)	$\tau_{cr,L}/\tau_y$ (18)	$\tau_{cr,G}/\tau_y$ (19)	τ_e/τ_{cr} (20)	τ_n/τ_y (21)	τ_e/τ_n (22)
1	82.73	620.52	358.3	0.968	0.953	1.000	1.016	0.690	1.404
2	71.17	637.76	368.2	0.808	0.943	1.000	0.856	0.686	1.177
3	50.04	675.68	390.1	0.660	0.693	1.000	0.953	0.570	1.159
4	87.63	665.34	384.1	0.979	0.900	1.000	1.088	0.669	1.464
5	93.41	618.32	357.0	0.939	0.692	1.000	1.356	0.569	1.649
6	119.47	678.58	391.8	0.878	0.885	1.000	0.992	0.663	1.325
7	74.73	591.50	341.5	0.754	0.785	1.000	0.960	0.618	1.220
8	96.17	613.84	354.4	0.806	0.902	1.000	0.893	0.670	1.203
9	75.57	591.50	341.5	0.572	0.785	0.777	0.736	0.552	1.035
10	133.35	587.84	339.4	0.819	0.986	0.835	0.981	0.637	1.285
11	46.26	665.34	384.1	0.627	0.568	1.000	1.105	0.494	1.270
12	72.50	665.34	384.1	0.789	0.840	1.000	0.940	0.643	1.227
13	43.28	620.52	358.3	0.587	0.700	1.000	0.838	0.574	1.023
14	61.20	637.76	368.2	0.697	0.855	1.000	0.815	0.650	1.073
15	61.83	577.84	333.6	0.665	0.612	1.000	1.086	0.522	1.274
16	97.86	605.98	349.9	0.803	0.854	1.000	0.940	0.650	1.236
17	56.49	551.58	318.5	0.611	0.696	1.000	0.878	0.571	1.070
18	93.41	596.05	344.1	0.806	0.833	1.000	0.968	0.640	1.260
19	77.26	609.63	352.0	0.591	0.580	0.960	1.018	0.497	1.189
20	126.72	638.66	368.7	0.740	0.832	0.992	0.889	0.638	1.160
21	41.14	665.34	384.1	0.549	0.315	1.000	1.745	0.300	1.830
22	61.16	641.21	370.2	0.695	0.484	1.000	1.435	0.436	1.594
23	34.47	703.26	406.0	0.435	0.298	1.000	1.462	0.285	1.526
24	53.38	561.92	324.4	0.587	0.769	1.000	0.764	0.609	0.963
25	31.14	713.60	412.0	0.387	0.293	1.000	1.321	0.281	1.376
26	48.93	634.31	366.2	0.564	0.487	1.000	1.159	0.437	1.289
27	51.60	551.58	318.5	0.594	0.330	1.000	1.799	0.313	1.895
28	80.06	602.39	347.8	0.672	0.476	1.000	1.411	0.430	1.563
29	52.93	689.47	398.1	0.477	0.275	1.000	1.733	0.265	1.797
30	78.64	579.98	334.9	0.686	0.495	1.000	1.386	0.443	1.547
31	69.08	673.27	388.7	0.468	0.294	1.000	1.594	0.282	1.662
32	101.46	584.26	337.3	0.648	0.508	1.000	1.275	0.453	1.430
33	63.16	572.26	330.4	0.888	1.000	1.000	0.888	0.707	1.256
34	55.16	668.79	386.1	0.741	1.000	0.969	0.765	0.696	1.065
35	57.82	586.05	338.4	0.786	1.000	1.000	0.786	0.707	1.111
36	57.82	620.52	358.3	0.799	1.000	1.000	0.799	0.707	1.130
37	80.95	689.47	398.1	0.796	1.000	0.475	1.675	0.429	1.855
38	88.78	592.12	341.9	0.932	1.000	0.578	1.612	0.500	1.862
39	82.29	618.25	356.9	0.827	1.000	0.553	1.494	0.484	1.708
40	77.62	558.82	322.6	0.846	1.000	0.619	1.367	0.526	1.607
41	70.77	605.98	349.9	0.533	1.000	0.321	1.661	0.306	1.745
42	79.31	620.52	358.3	0.572	1.000	0.317	1.806	0.302	1.895

Table 2. European tests (Lindner and Aschinger 1988; Peil 1998).

ID	Specimen	a	h_w	t_w	b	d	h_r	α	β	w/t_w	$F(\alpha,\beta)$
		(mm)	(mm)	(mm)	(mm)	(mm)	(mm)	(deg.)			
(1)	(2)	(3)	(4)	(5)	(6)	(7)	(8)	(9)	(10)	(11)	(12)
43	L1A	977	994	1.94	140	50	50	45	1.98	72	0.42
44	L1B	982	994	2.59	140	50	50	45	1.98	54	0.42
45	L2A	1498	1445	1.94	140	50	50	45	1.98	72	0.42
46	L2B	1497	1445	2.54	140	50	50	45	1.98	55	0.42
47	L3A	2004	2005	2.01	140	50	50	45	1.98	70	0.42
48	L3B	2004	2005	2.53	140	50	50	45	1.98	55	0.42
49	B1	800	600	2.1	140	50	50	45	1.98	67	0.42
50	B4	800	600	2.11	140	50	50	45	1.98	66	0.42
51	B4b	800	600	2.11	140	50	50	45	1.98	66	0.42
52	B3	800	600	2.62	140	50	50	45	1.98	53	0.42
53	B2	700	600	2.62	140	50	50	45	1.98	53	0.42
54	M101	600	600	0.99	70	15	15	45	3.30	71	0.21
55	M102	800	800	0.99	70	15	15	45	3.30	71	0.21
56	M103	1000	1000	0.95	70	15	15	45	3.30	74	0.21
57	M104	1200	1200	0.99	70	15	15	45	3.30	71	0.21
58	L1	1497	1000	2.1	106	86.6	50	30	1.06	50	0.57
59	L1	1492	1000	3	106	86.6	50	30	1.06	35	0.57
60	L2	2150	1498	2	106	86.6	50	30	1.06	53	0.57
61	L2	2148	1498	3	106	86.6	50	30	1.06	35	0.57
62	No. 1	1133	850	2	102	85.5	55.5	33	1.00	51	0.70
63	No. 2	1133	850	2	91	71.5	56.3	38.2	1.00	46	0.87
64	V1/1	2820	298	2.05	144	102	102	45	1.00	70	1.08
65	V1/2	2000	298	2.1	144	102	102	45	1.00	69	1.08
66	V1/3	1000	298	2	144	102	102	45	1.00	72	1.08
67	V2/3	1650	600	3	144	102	102	45	1.00	48	1.08
68	SP1	1750	800	2	146	104	104	45	0.99	74	1.09
69	SP2	1750	800	2	170	80	80	45	1.50	85	0.62
70	SP3	1750	800	2	185	65	65	45	2.01	93	0.41
71	SP4	1800	800	2	117	83	83	45	1.00	59	1.09
72	SP5	1800	800	2	136	64	64	45	1.50	68	0.62
73	SP6	1800	800	2	148	52	52	45	2.01	74	0.41
74	SP2-2-400 1	1000	400	2	170	80	80	45	1.50	85	0.62
75	SP2-2-400 2	1000	400	2	170	80	80	45	1.50	85	0.62
76	SP2-2-800 1	1000	800	2	170	80	80	45	1.50	85	0.62
77	SP2-2-800 2	1000	800	2	170	80	80	45	1.50	85	0.62
78	SP2-3-600 1	1000	600	3	170	80	80	45	1.50	57	0.62
79	SP2-3-600 2	1000	600	3	170	80	80	45	1.50	57	0.62
80	SP2-3-1200 1	1000	1200	3	170	80	80	45	1.50	57	0.62
81	SP2-3-1200 2	1000	1200	3	170	80	80	45	1.50	57	0.62
82	SP2-4-800 1	1000	800	4	170	80	80	45	1.50	43	0.62
83	SP2-4-800 2	1000	800	4	170	80	80	45	1.50	43	0.62
84	SP2-4-1600 1	1000	1600	4	170	80	80	45	1.50	43	0.62
85	SP2-4-1600 2	1000	1600	4	170	80	80	45	1.50	43	0.62
86	SP2-8-800 1	1000	800	8	170	80	80	45	1.50	21	0.62
87	SP2-8-800 2	1000	800	8	170	80	80	45	1.50	21	0.62

Table 2. European tests (Lindner and Aschinger 1988; Peil 1998) (continued).

ID	V_e (kN)	F_y (MPa)	τ_y (MPa)	τ_e/τ_y	$\tau_{cr,L}/\tau_y$	$\tau_{cr,G}/\tau_y$	τ_e/τ_{cr}	τ_n/τ_y	τ_e/τ_n
(13)	(14)	(15)	(16)	(17)	(18)	(19)	(20)	(21)	(22)
43	280	292	169	0.861	0.938	1.000	0.918	0.684	1.259
44	502	335	193	1.008	1.000	1.000	1.008	0.707	1.426
45	337	282	163	0.738	0.954	1.000	0.774	0.690	1.069
46	564	317	183	0.840	1.000	1.000	0.840	0.707	1.187
47	450	280	162	0.691	0.992	0.803	0.860	0.624	1.106
48	775	300	173	0.882	1.000	0.822	1.073	0.635	1.389
49	208	341	197	0.838	0.939	1.000	0.893	0.685	1.225
50	183	363	210	0.690	0.915	1.000	0.754	0.675	1.022
51	217	363	210	0.818	0.915	1.000	0.894	0.675	1.212
52	246	317	183	0.855	1.000	1.000	0.855	0.707	1.209
53	273	315	182	0.955	1.000	1.000	0.955	0.707	1.350
54	53	189	109	0.818	1.000	1.000	0.818	0.707	1.156
55	79	190	110	0.909	1.000	0.850	1.070	0.647	1.404
56	84	213	123	0.719	1.000	0.505	1.425	0.451	1.596
57	104	189	109	0.802	1.000	0.403	1.990	0.374	2.145
58	380	410	237	0.764	1.000	1.000	0.764	0.707	1.081
59	610	450	260	0.783	1.000	1.000	0.783	0.707	1.107
60	600	376	217	0.923	1.000	0.872	1.058	0.657	1.404
61	905	402	232	0.868	1.000	0.933	0.930	0.682	1.272
62	275	355	205	0.789	1.000	1.000	0.789	0.707	1.116
63	265	349	201	0.774	1.000	1.000	0.774	0.707	1.094
64	68	298	172	0.647	0.952	1.000	0.680	0.690	0.938
65	70	283	163	0.685	1.000	1.000	0.685	0.707	0.968
66	81	298	172	0.790	0.929	1.000	0.850	0.681	1.161
67	235	279	161	0.810	1.000	1.000	0.810	0.707	1.146
68	225.00	306.5	177	0.795	0.898	1.000	0.885	0.668	1.189
69	215.30	298.5	172	0.781	0.775	1.000	1.007	0.613	1.274
70	209.50	291.5	168	0.778	0.670	1.000	1.161	0.557	1.397
71	230.80	297.5	172	0.840	1.000	1.000	0.840	0.707	1.188
72	220.50	290.5	168	0.822	0.998	1.000	0.823	0.706	1.163
73	220.00	293.5	169	0.811	0.912	1.000	0.889	0.674	1.204
74	80.25	262.5	152	0.662	0.840	1.000	0.788	0.643	1.029
75	88.13	262.5	152	0.727	0.840	1.000	0.866	0.643	1.130
76	178.88	272	157	0.712	0.825	1.000	0.863	0.636	1.119
77	177.75	272	157	0.707	0.825	1.000	0.858	0.636	1.112
78	301.50	294	170	0.987	1.000	1.000	0.987	0.707	1.396
79	308.63	294	170	1.010	1.000	1.000	1.010	0.707	1.429
80	611.25	294	170	1.000	1.000	1.000	1.000	0.707	1.415
81	625.13	294	170	1.023	1.000	1.000	1.023	0.707	1.447
82	601.50	325.5	188	1.000	1.000	1.000	1.000	0.707	1.415
83	603.38	325.5	188	1.003	1.000	1.000	1.003	0.707	1.419
84	1215.38	328	189	1.003	1.000	1.000	1.003	0.707	1.418
85	1227.00	328	189	1.012	1.000	1.000	1.012	0.707	1.432
86	1308.38	269.5	156	1.314	1.000	1.000	1.314	0.707	1.858
87	1374.75	269.5	156	1.381	1.000	1.000	1.381	0.707	1.952

A plot of the normalized shear stress capacity, τ / τ_y, versus the normalized web slenderness ratio is given in Figure 3, where, for each test where local buckling controls the shear behavior (*i.e.*, $(\tau_{cr,L})_{el} < (\tau_{cr,G})_{el}$) and the global buckling stress (from Equation 5) is the yield stress (*i.e.*, $\tau_{cr,G} / \tau_y = 1$), τ_e / τ_y is plotted. The theoretical lower bound results from Equations 1 and 5 are also plotted as τ_{cr} / τ_y. Figure 3 shows that the theoretical lower bound curve safely estimates the local buckling strength for most of the slender web cases where the behavior is controlled, in theory, by elastic buckling (*i.e.*, Equation 1). However, with decreasing web slenderness, the theoretical lower bound tends to overestimate the test results especially for webs where the behavior is controlled, in theory, by inelastic buckling or yield (*i.e.*, Equation 5). It is thus concluded that Equations 1 and 5 should not be used to estimate the nominal shear strength of bridge girders with corrugated webs.

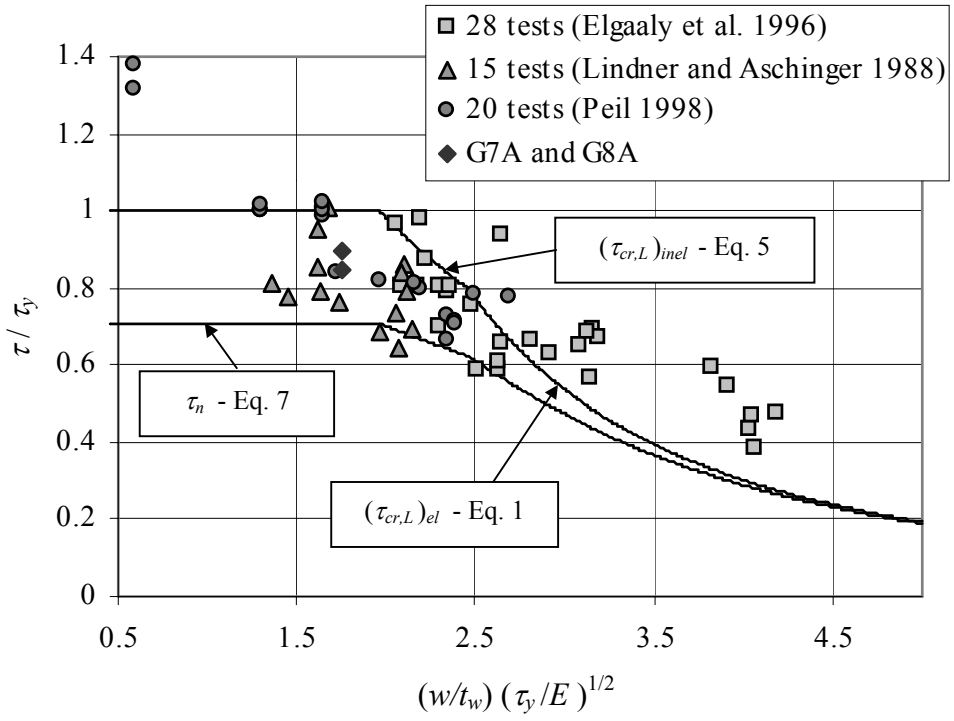

Figure 3. Comparison of calculated shear strength with test results.

2.3. Proposed Nominal Shear Strength Equation

To date, a clear explanation of the discrepancy between the theoretical and the experimental results in Figure 3 has not been given in the literature. However, as discussed later, geometric imperfections (out-of-flatness) of the folds of corrugated webs may be an important factor. Until further research on this issue is completed, the

following equation for the nominal shear strength, τ_n, is proposed for use in the design of bridge girders with corrugated webs:

$$\tau_n = \sqrt{\frac{(\tau_{cr,L} \cdot \tau_{cr,G})^2}{\tau_{cr,L}^2 + \tau_{cr,G}^2}} \tag{7}$$

In Equation 7, local and global buckling capacities are calculated from Equations 1, 3, or 5 using the lower bound values for k_L and k_G. Equation 7 is derived from an elastic interaction buckling formula investigated by Lindner and Aschinger (1988). Here, Equation 7 is suggested for use over the entire range of behavior, including the cases where elastic buckling, inelastic buckling, or yield control the local and global buckling behavior. Equation 7 is graphically represented in Figure 3 assuming that local buckling controls the shear behavior, and the global buckling stress (from Equation 5) is the yield stress, τ_y. Figure 3 shows that Equation 7 is a reasonable lower bound for the test results where local buckling controls the shear behavior.

The ratio τ_e / τ_n of column 22 in Tables 1 and 2 compares the test results (τ_e) with the results from Equation 7 (τ_n). When the ratio τ_e / τ_n exceeds 1, Equation 7 provides a conservative estimate of the test results. Figure 4 plots τ_e / τ_n versus the ratio $\tau_{cr,G} / \tau_y$ for all tests. The cases when $\tau_{cr,G} / \tau_y = 1$, are the cases plotted above in Figure 3, where local buckling controls the shear behavior. For the cases when $\tau_{cr,G} / \tau_y < 1$, the shear behavior may be controlled by either local or global buckling. For all cases, Figure 4 shows that Equation 7 is a reasonable lower bound to the test results.

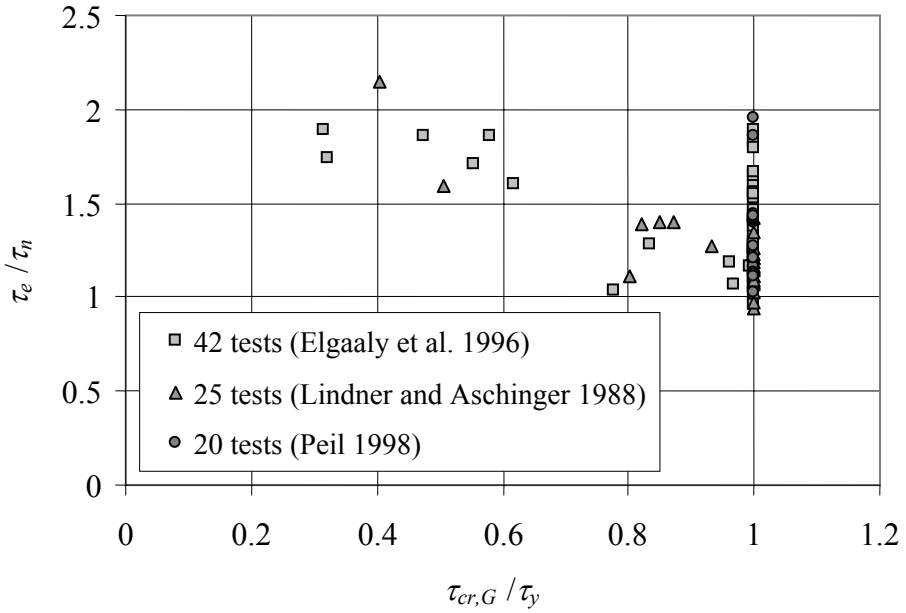

Figure 4. Comparison of shear strength from Equation 7 with test results.

3. Shear Strength Tests of Corrugated Web Girders

Two full-scale corrugated web girder specimens (Figure 5), designated Girder G7A and Girder G8A, were designed, fabricated, and tested to failure in shear under monotonically increasing load. The objective of these tests was to assess the proposed equation for the nominal shear strength, τ_n, given as Equation 7. The shear strength test specimens were made identical in nominal geometry and material in order to study the effect of web geometric imperfections on the shear strength.

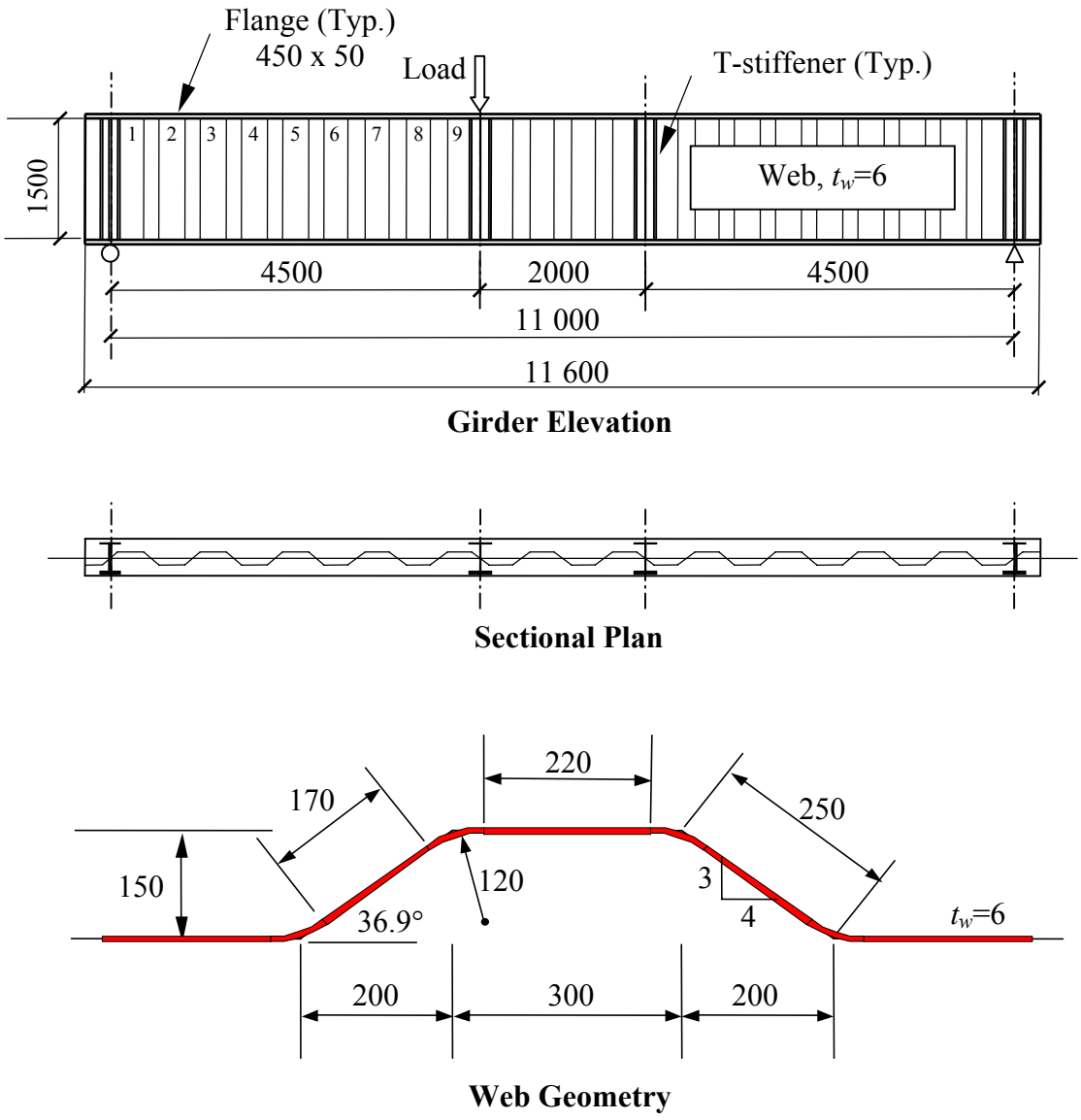

Note: dimensions are measured to middle surface of web plate

Figure 5. Corrugated web shear test specimens (dimensions in mm).

3.1. Design and Fabrication of Test Specimens

The test specimens were designed with a full-scale trapezoidal web profile (Figure 5). The nominal web thickness of 6mm (1/4in) and the trapezoidal web profile are identical to those selected for the demonstration bridge, as discussed in Section 7. The nominal web depth of 1500mm (59.1in) maximized the web depth (to fully validate the results from Equation 7) without making the failure load and reactions excessive. For example, based on the nominal web thickness and depth, and the nominal yield stress of HPS-485W, the shear force needed to yield the web was estimated to be 2520kN (566kips). The 6mm (1/4in) thick web with a web depth of 1500mm (59.1in) (*i.e.*, with $h_w/t_w = 250$) and the corrugation geometry shown in Figure 5, was expected to reach the yield stress for both local buckling (Equations 1 and 5) and global buckling (Equations 3 and 5).

The two specimens were tested as simply supported beams with a span of 11m (36.1ft). The load was applied 1m (39.4in) from midspan to force the shear failure to occur in the shorter shear span. Based on this test configuration and the expected shear yield force of 2520kN (566kips), the applied force needed to yield the specimens in shear was estimated to be 4260kN (957kips). To prevent web crippling and to maintain cross section geometry under these large concentrated forces, T-stiffeners were provided at the reactions and load points. To reduce the potential that tension field action or flange frame action would carry significant levels of shear, the test configuration provided a shear span-to-web depth ratio of three in the shorter shear span.

The flanges were designed so that the ratio of the shear yield load, P_{Vy}, to the moment yield load, P_{My}, was approximately 70%. P_{My} was calculated neglecting the contribution of the web. P_{Vy} was calculated assuming that the shear is carried entirely by the web. The variation of bending moment within the failure shear span from low (near the support) to high (near the load point), provided an opportunity to assess the possibility that moment-shear interaction would influence the shear strength.

The shear test specimens were fabricated by High Steel Structures, Inc. from ASTM A709, grade HPS-485W steel (Sause 2003). Tension coupon tests of the flange and web material were conducted. The average measured yield stress of the flange material was 499MPa (73.4ksi). The average measured yield stress of the web material was 466MPa (67.6ksi) for girder G7A and 464MPa (67.3ksi) for girder G8A. These yield stress values (from the 0.2% offset method) are less than the minimum specified, however at a strain slightly beyond the 0.2% offset strain, the stress was above the minimum of 485MPa (Abbas 2003). The thickness of the web plate was 6.30mm (0.248in) for girder G7A and 6.27mm (0.247in) for girder G8A, greater than the expected 6mm (0.236in).

Using a special die, a brake-press process was used to cold form the trapezoidal web corrugations. A large bend radius of 120 mm (4.72 in.) (Figure 5) was used for reasons discussed by Sause *et al.* (2003). Web-to-flange fillet welds were made using a gas metal arc welding (GMAW) process. Stiffener-to-web fillet welds were made using a flux-cored arc welding (FCAW) process. Web splices were made using either the GMAW or the submerged arc welding (SAW) process (Sause 2003).

3.2. Finite Element Analyses of Test Specimens

A finite element (FE) model of the shear test specimens (Figure 6) was developed (Abbas 2003). The general purpose FE package ABAQUS (Hibbitt *et al*. 1998) was used. The model was used to perform a linear elastic eigenvalue buckling analysis and nonlinear inelastic load-deflection buckling analyses. The FE model was simply supported and loaded as shown in Figure 5. The steel elastic material properties were the elastic modulus, E, equal to 200,000MPa (29,000ksi), and Poisson's ratio, ν, equal to 0.3. For the nonlinear inelastic analyses, an elastic-perfectly-plastic stress-strain curve, with a yield strength of 485MPa (70.3ksi), was used to idealize the HPS-485W steel used in the web and flanges. A von Mises yield criterion with the associated flow rule was used to model the elasto-plastic behavior of the steel.

A linear elastic eigenvalue buckling analysis of the FE model was conducted. The lowest 50 (positive) buckling loads (eigenvalues) and the corresponding buckling shapes (eigenmodes) were determined. The lowest buckling load corresponded to a lateral torsional buckling mode, which was ignored because it would be restrained during the shear tests. The remaining 49 buckling loads and corresponding buckling shapes were observed to be shear buckling modes involving local buckling of the longitudinal folds. Figure 6 shows the 1st and the 49th shear buckling modes. It is observed that local shear buckling occurs in the longitudinal folds, involving several folds simultaneously. This behavior is expected because the longitudinal folds all have the same slenderness and nominal shear stress.

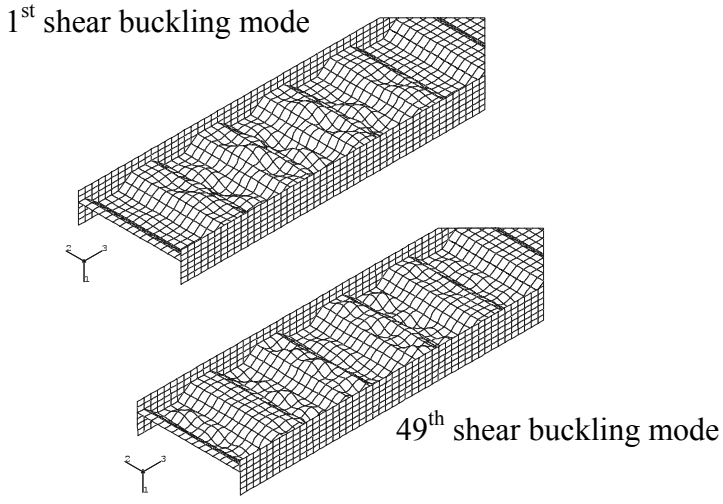

Figure 6. Shear buckling modes from FE analysis of shear test specimens.

The shear buckling stresses from the 49 shear buckling modes were divided by the ratio on the right hand of Equation 1 ($((\pi^2 E)/(12\,(1-\nu^2)(w/t_w)^2)$) to express the buckling loads as an effective buckling coefficient, k_L. The values of E equal to 200,000MPa (29,000ksi), ν equal to 0.3, w equal to 300mm (11.8in), and t_w equal to 6mm (1/4in), were based on the nominal material and geometry of the shear test specimens (Figure 5).

Figure 7 shows that the effective k_L values are rather closely spaced, especially for the first few modes. Furthermore, a k_L value of 6.38 for the 1st shear mode indicates that the inclined folds (with a nominal width of 250mm (9.84in)) provide the more critical longitudinal folds (with a nominal width of 300mm (11.8in)) with boundary conditions that lie between simply supported (k_L = 5.34) and fixed (k_L = 8.98). Figure 6 shows that the inclined folds have deformations that are compatible with those in the adjacent longitudinal folds, suggesting that the inclined fold deformations are a result of partial restraint of the longitudinal fold deformations along the interface between the folds.

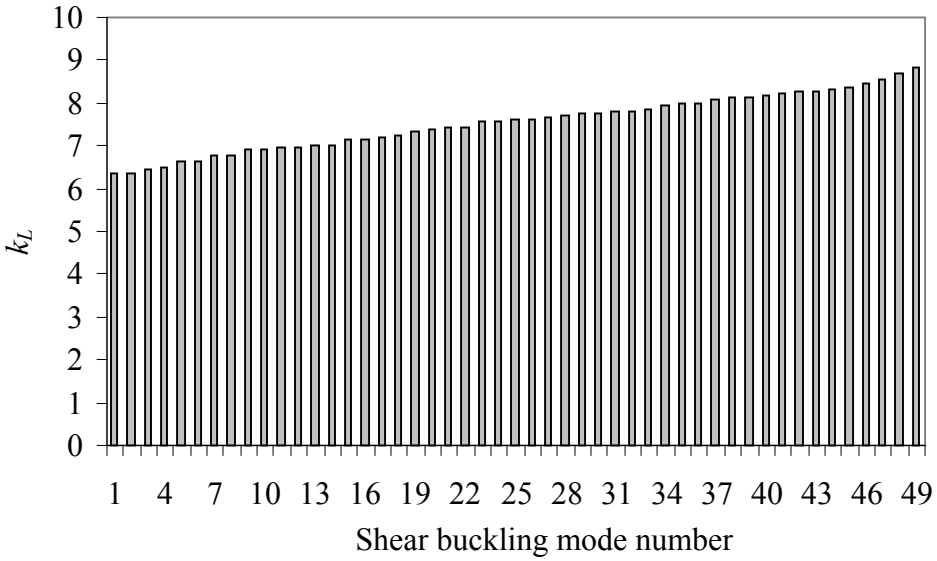

Figure 7. Shear buckling coefficients from FE analysis of shear test specimens.

To study the effect of web geometric imperfections on the shear strength, nonlinear inelastic load-deflection buckling analyses of the FE model (including both geometric and material nonlinearity) were performed using the modified Riks method available in ABAQUS (Abbas 2003). The FE model was similar to the model used in the linear elastic analyses, except that the load point was laterally restrained to eliminate the lateral torsional buckling mode, and small changes in the geometry were introduced to simulate geometric imperfections. The initial geometric imperfections were introduced by scaling the geometry of the buckling modes from the linear elastic buckling analysis and adding the scaled buckling mode geometry to the original (perfect) geometry.

Assuming that the 1st shear buckling mode is more critical than the other modes, the 1st mode was used for the first geometric imperfection study. This study considered the effect of imperfection amplitude on the shear strength. Figure 8 shows the normalized shear stress capacity versus the normalized web imperfection amplitude, which is the amplitude of the web imperfection (out-of-flatness) divided by the web thickness, t_w. The figure shows that for small imperfections (up to approximately 10% of t_w, *i.e.*, 0.6 mm) the shear stress capacity approaches the shear yield stress. As the web imperfection

amplitude increases, a decrease in shear stress capacity occurs. For a normalized imperfection amplitude of 100% (*i.e.*, 6mm (1/4in)), the shear stress capacity is only 76.6% of the shear yield stress. Greater imperfections will lead to further decreases, and it is therefore concluded that the shear buckling strength is imperfection sensitive.

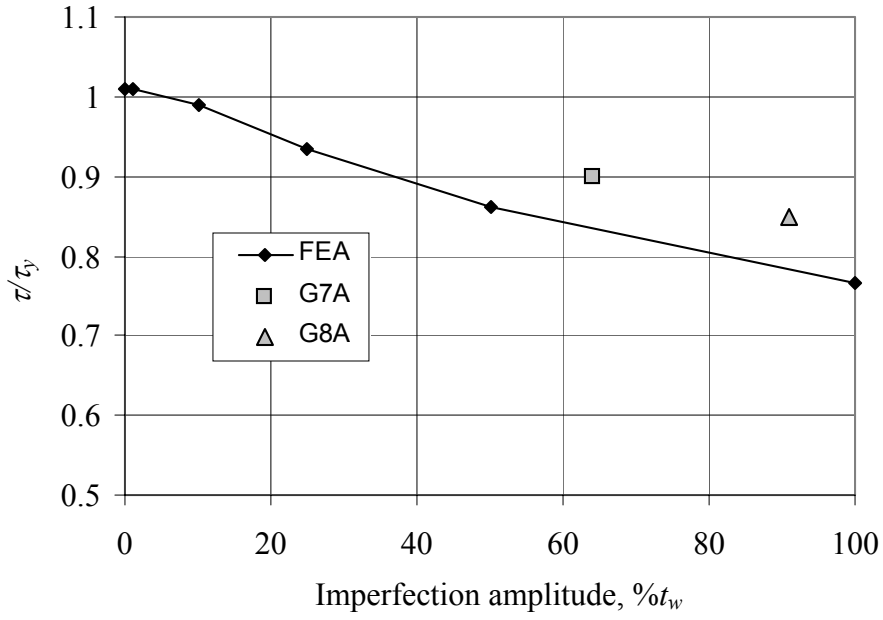

Figure 8. Shear stress capacity from FE analysis versus imperfection amplitude.

The second geometric imperfection study considered the effect of imperfection shape on the shear strength. The imperfection amplitude was kept constant at 100% t_w, as the elastic shear buckling modes from the linear elastic buckling analysis were considered as the imperfection shape. Figure 9 shows the normalized shear stress capacity as different elastic shear buckling modes are considered as the imperfection shape. The figure shows that the general trend is for the shear stress capacity to increase with the mode number.

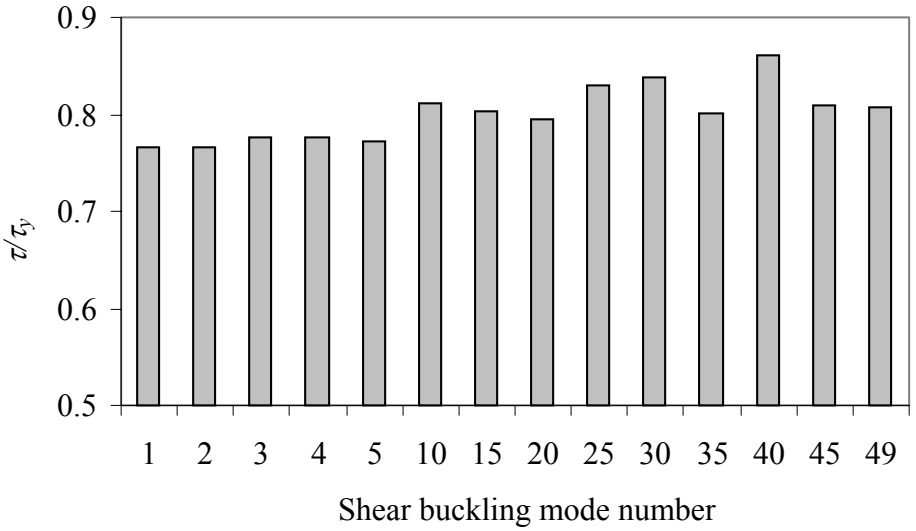

Figure 9. Shear stress capacity from FE analysis versus imperfection shape.

3.3. Measurement of Specimen Imperfections and Preliminary Tests

The finite element analyses illustrated the importance of web initial out-of-flatness geometric imperfections. Therefore, two tasks were undertaken prior to the shear strength tests: (1) measurement of web initial out-of-flatness imperfections (without applied load), and (2) measurement of the growth in web out-of-flatness (web out-of-plane deflections) under applied load. As shown in Figure 5, the shear test specimens were simply supported with the load applied to force shear failure in the shorter shear span. Web initial out-of-flatness imperfections were measured on the nine longitudinal folds within this shorter shear span (i.e., Folds 1 to 9 shown in Figure 5).

The web initial out-of-flatness imperfections were measured using two methods, a manual method and an automated method. In the manual method, an approximately 1450mm (57in) long aluminum straight edge was placed against the web surface down the middle of each longitudinal fold. The gap between the web and the straight edge, resulting from the web out-of-flatness, was then measured at various locations over the height of the web. This process was repeated for Folds 1 to 9. The results indicate that the web was bent primarily in single curvature with the center of curvature toward the near side of the girder (where the web is closest to the flange tip) as shown in Figure 10.

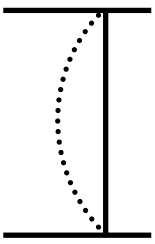

Figure 10. Schematic of web initial out-of-flatness geometric imperfections.

A plot of web depth versus web initial out-of-flatness geometric imperfection for Folds 1 to 9 of Girders G7A and G8A is shown in Figure 11. The maximum measured imperfection amplitude was approximately 6mm (1/4in).

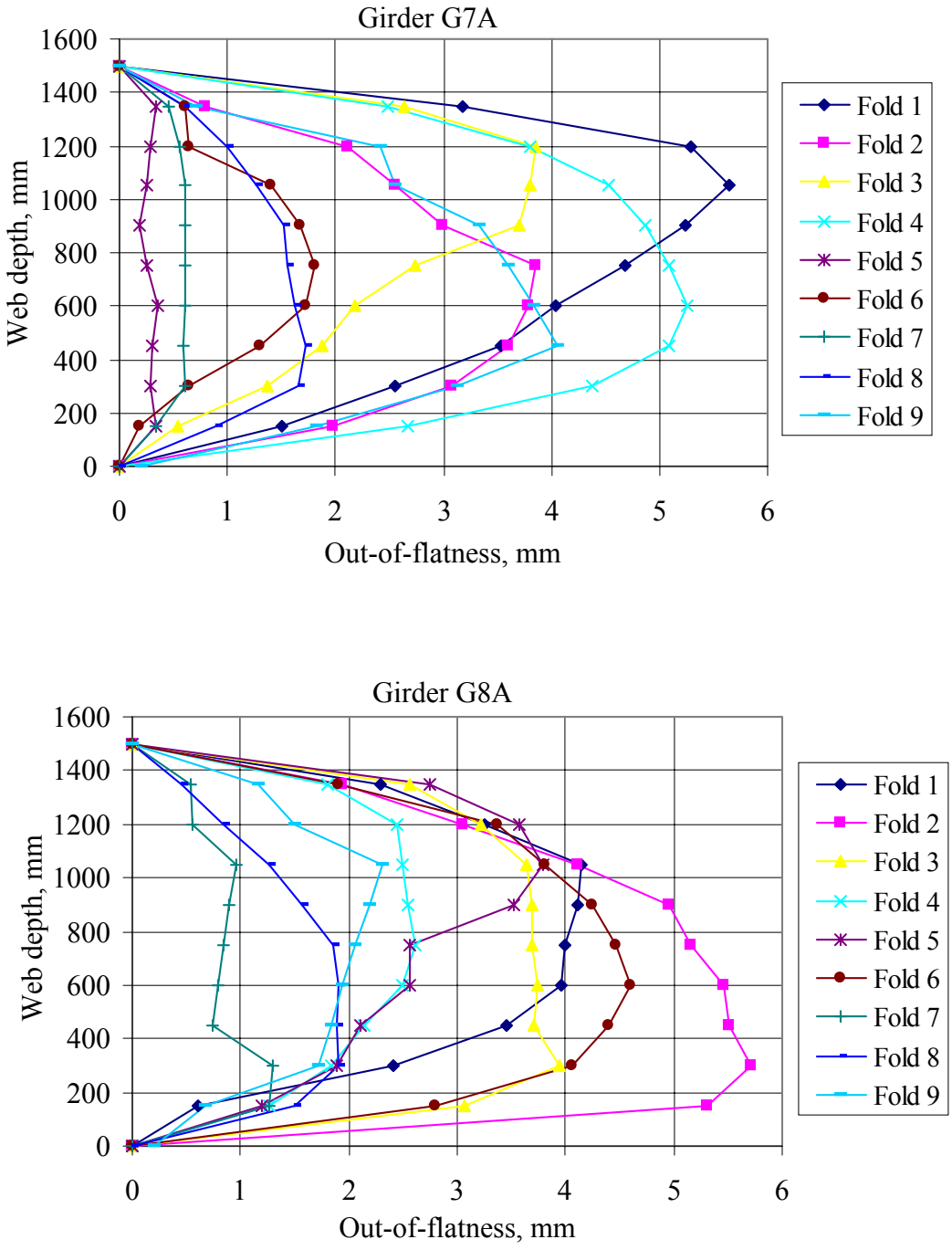

Figure 11. Measured web geometric imperfections for Girders G7A and G8A.

To verify the manually measured results, specially-made web deflection measurement rigs, shown in Figure 12, were used to make automated measurements. The rigs were made to measure web out-of-plane deflections under loading, however, it was possible to use them to measure the initial web out-of-flatness. Each rig (a total of five rigs were made) consisted of an aluminum angle with a magnet on each end of the angle to secure the rig to the web surface. Each rig had up to nine equally spaced displacement potentiometers along the length of the rig. The displacement potentiometers were spring loaded so that the plunger of the sensor could maintain contact with the web. The recorded relative movement between the web and the rig indicated web out-of-plane deflection.

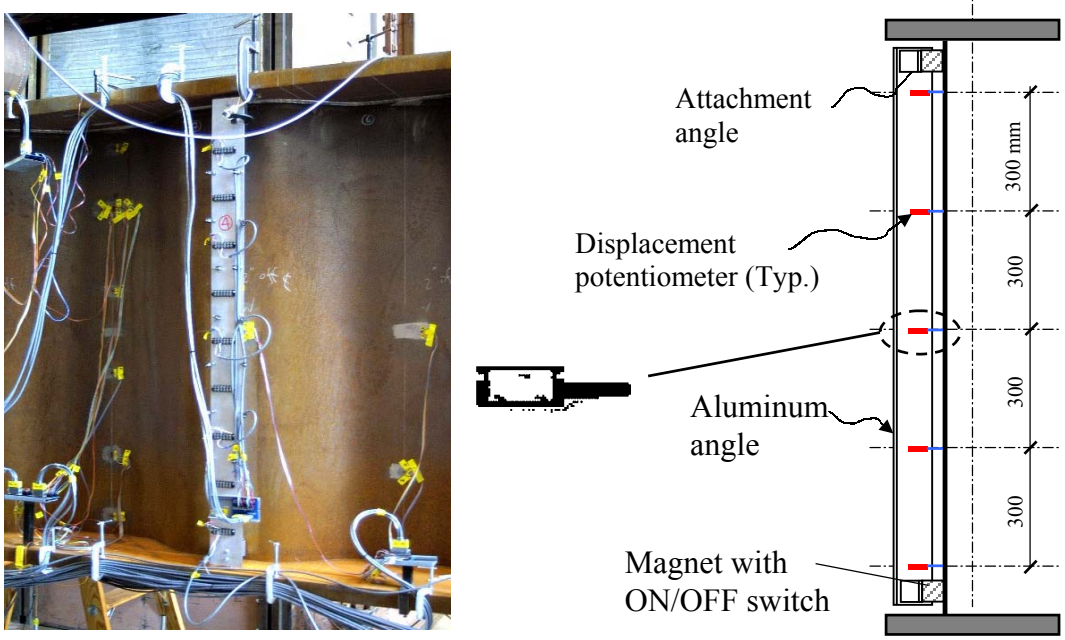

Figure 12. Web fold deflection measurement rig.

To use a web deflection measurement rig to make automated measurements of the web initial out-of-flatness geometric imperfections, the rig was first placed on a perfectly flat surface and an initial set of readings was electronically recorded. Then, the rig was carefully mounted on the web and a second set of readings was taken. The difference between both readings gave the web initial out-of-flatness.

Figure 13 shows good agreement between the results obtained for Girder G7A using the two measurement methods. It is important to note that the reference line for web imperfections is a straight line that passes through the two points where the ends of the straight edge (or the magnets of a deflection rig) are in contact with the web near the middle of each longitudinal fold. Therefore, only the web initial out-of-flatness down the middle of the longitudinal fold is measured.

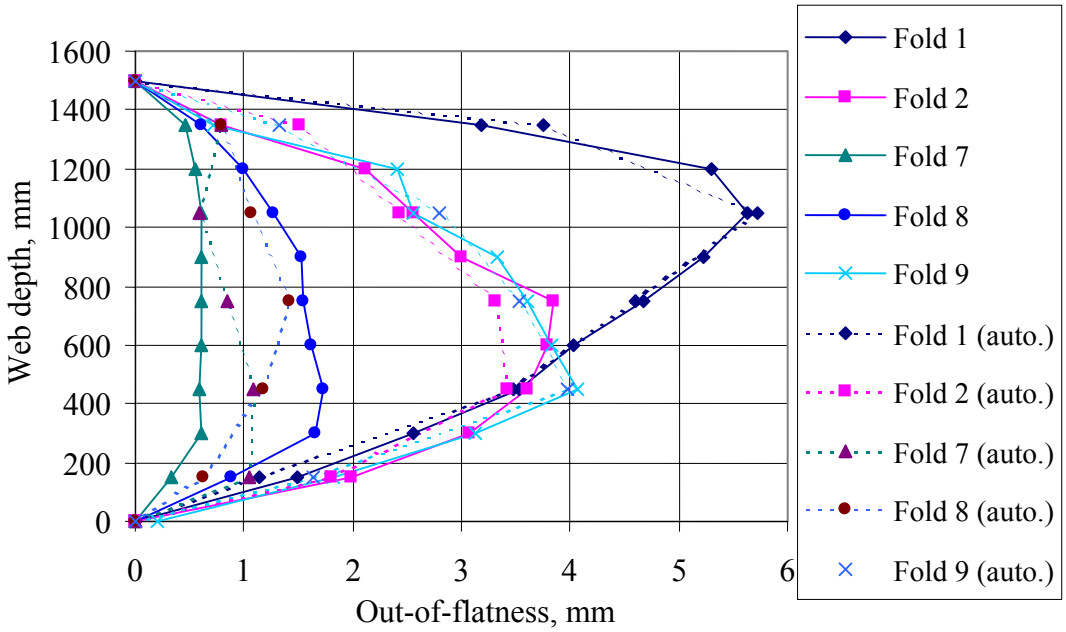

Figure 13. Manual and automated measurements of web geometric imperfections.

The second task undertaken prior to the shear strength tests was the measurement of web out-of-plane deflections under loading. Girder G7A and Girder G8A were loaded to a relatively low load level of approximately 1335kN (300kips) to ensure elastic behavior. Web deflection measurement rigs with five sensors per rig were used. No other sensors were used. The objective was to determine which longitudinal folds were more critical for local buckling due to growth in initial imperfections. This information was considered to be important because, theoretically, all nine longitudinal folds (i.e., Folds 1 to 9) within the shorter shear span of the test specimens (Figure 5) were possible locations of shear buckling during the tests to failure.

Figure 14 shows the results of web out-of-plane deflections for Fold 8 of Girder G7A at various load levels. Observe that this particular fold deflects in double curvature, despite the fact that the pattern of initial geometric imperfections was in single curvature. Folds that deflect in double curvature under loading are considered to be more likely to locally buckle in shear than folds that deflect in single curvature.

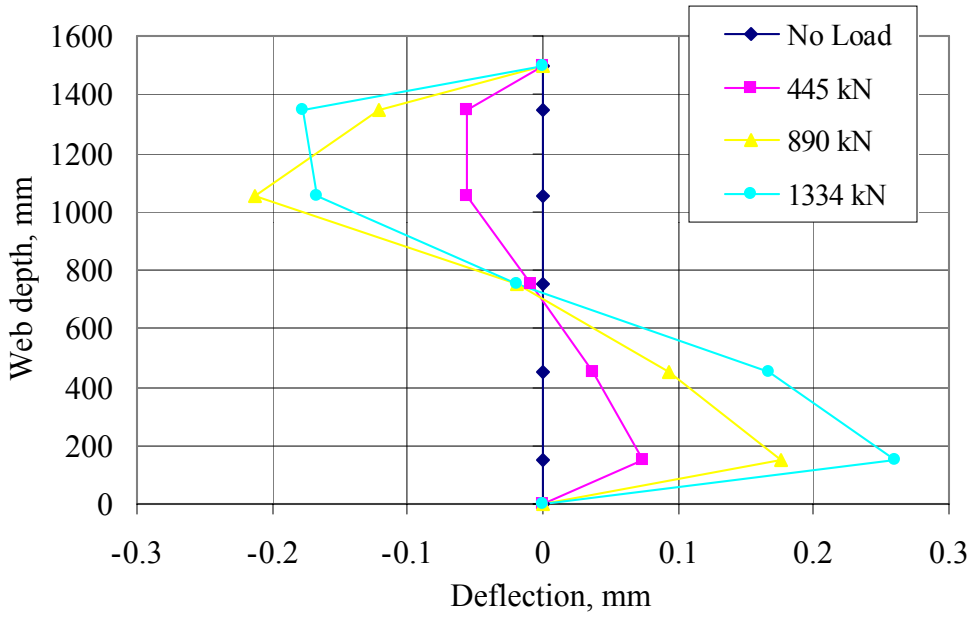

Figure 14. Web out-of-plane deflections under loading for Fold 8 of Girder G7A.

3.4. Set-up and Instrumentation for Shear Strength Tests

The shear strength tests were performed under the five million pound universal testing machine in Fritz Engineering Laboratory at Lehigh University (Figure 15).

Figure 15. Test specimen in five million pound universal testing machine.

In order to prevent lateral-torsional buckling, two lateral braces, one on each side of the test specimen, were provided at approximately 700mm (28in) from the load point. Each brace was designed to transfer lateral forces by contact from the top flange of the test specimen through a horizontal steel member to the legs of the testing machine as shown in Figure 16. Additionally, a laterally braced vertical steel member was provided for stability as shown in Figure 16. To minimize friction forces, 6mm (1/4in) thick Teflon sheets were glued on the contact surfaces of both the test specimen and the brace. An intentional gap of 6mm (1/4in) was left between the brace and the specimen before load application to eliminate friction forces in the early testing stages.

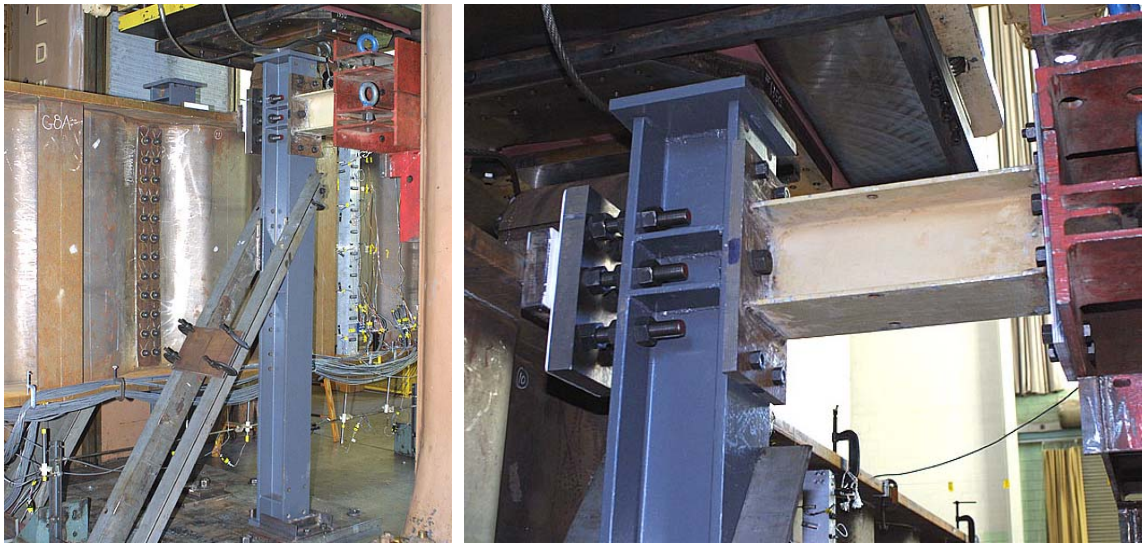

Figure 16. Lateral brace arrangement.

The simply supported boundary conditions at the ends of the test specimens were provided using high strength solid steel rollers (Figure 15). Each roller was placed between two 50mm (2in) thick steel plates over a stiffened steel pedestal. The west end roller at the end of the shorter shear span of the test set-up had a diameter of 290mm (11.5in) while the east end roller had a diameter of 250mm (10in). At the loading point, a hollow roller between two 50mm (2in) thick steel plates was used. The roller had an outside diameter of 500mm (20in) and an inside diameter of 70mm (2.75in). These large dimension rollers reduced the contact stresses and avoided local deformations that would hinder free movement in the longitudinal direction. Figure 15 shows that sets of slightly slack industrial slings were provided at the ends of the test set-up to restrain potential movements of the specimen at failure.

The test specimens were instrumented using a combination of strain gages, linear variable displacement transducers (LVDTs), and displacement potentiometers. The ATLSS modular large-scale data acquisition system running the commercially available software TestPoint was used acquire data. A total of 163 channels were used for each test specimen as follows: 116 channels for strain gages, 19 channels for LVDTs, 26 channels for displacement potentiometers, 1 channel for applied load, and 1 channel for machine head displacement.

3.5. Results and Observations from Shear Strength Tests

The test results for Girders G7A and G8A are shown on the load-deflection plots of Figures 17 and 18, respectively. Both girders failed suddenly by web buckling with a dynamic drop in load from point a to point b, as shown in Figures 17 and 18. The web went from an apparently intact configuration prior to failure, to a fully buckled configuration after failure.

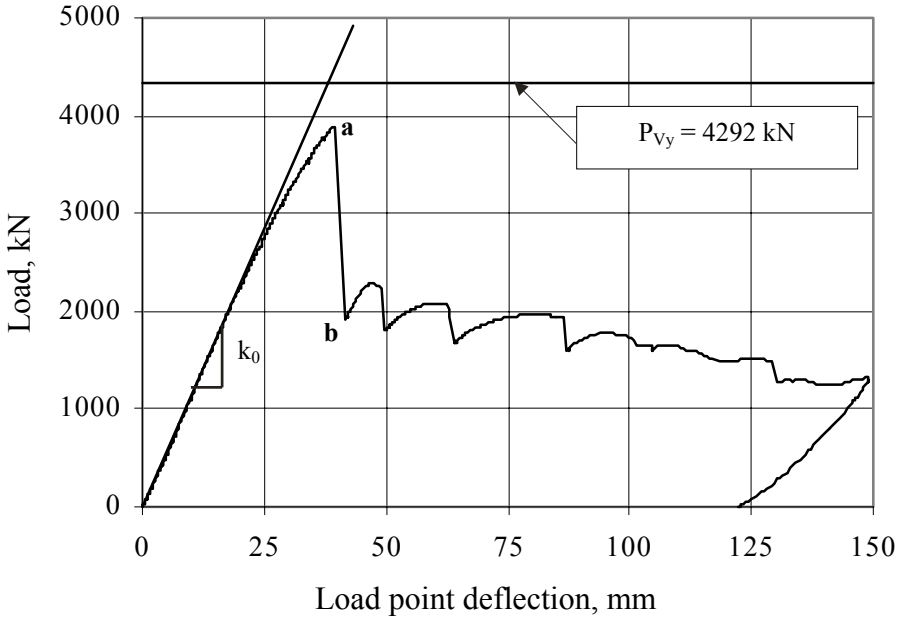

Figure 17. Load versus deflection for Girder G7A.

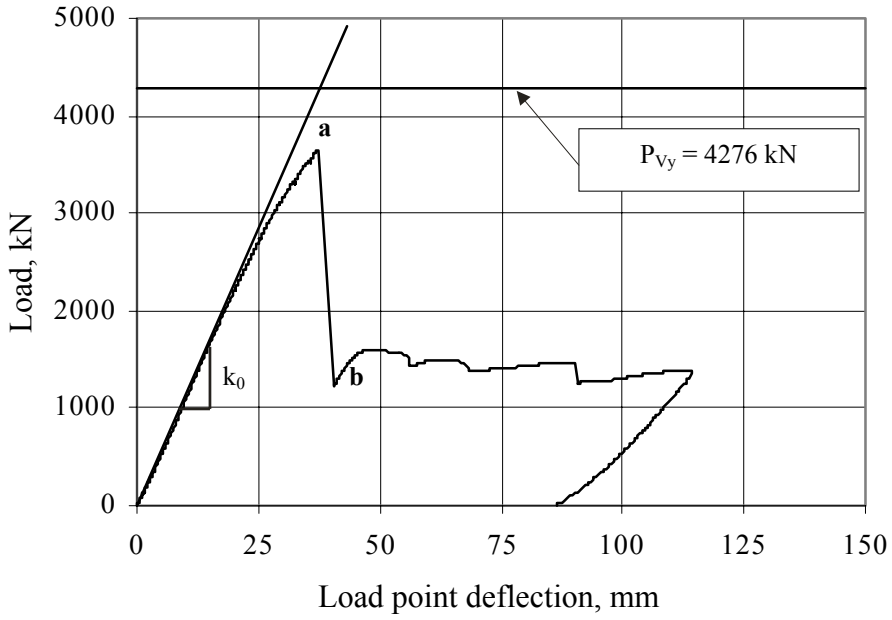

Figure 18. Load versus deflection for Girder G8A.

Girder G7A failed at a load level of 3892kN (875kips) with an instantaneous load drop to 1914kN (430kips). At the failure load, τ_e was 243MPa (35.2ksi), and the ratio τ_e / τ_y was 0.907. Web buckling occurred in the area involving Folds 7, 8, and 9 in the top half of the girder near the load point. The buckled waves, extending over parts of the inclined folds as well as the longitudinal folds, had different sizes and different angles of inclination with respect to the horizontal. The steepest wave involved Folds 8 and 9, and extended over approximately half the girder depth. The appearance of the failed web after the initial load drop (*i.e.*, at point b in Figure 17) is shown in Figure 19. As Girder G7A was pushed further, more folds buckled (one at a time from Fold 6 to Fold 3 towards the support), again near the top flange. The growing web deformations eventually became large enough to result in local tearing of the web at a few locations in the heat affected zone close to the web-to-flange weld. The test was terminated shortly afterwards.

Similarly, Girder G8A failed at a load level of 3647kN (820kips) with an instantaneous load drop to 1226kN (276kips). At the failure load, τ_e was 229MPa (33.2ksi), and the ratio τ_e / τ_y was 0.853. Unlike Girder G7A, Girder G8A failed by web buckling in the area involving Folds 2, 3, and 4 near the support. The buckled waves extended over the entire depth of the girder, all at an angle of approximately 45 degrees. The appearance of the failed web after the initial load drop (*i.e.*, at point b in Figure 18) is shown in Figure 20. As Girder G8A was pushed further, folding and stretching in the web gradually took place and more buckles appeared on Folds 5 and 6 near the bottom flange and on Fold 1 near the top flange. The fact that Girder G8A failed near the support away from the load point in a region of low bending stresses is in itself an indication that there is probably little interaction between bending and shear in the web.

Figure 19. Girder G7A after failure.

Figure 20. Girder G8A after failure.

3.6 Analysis and Discussion of Results from Shear Strength Tests

Due to the nature of the failure modes observed, a clear distinction between the pre-peak stage and the post-peak stage is made. The behavior prior to the peak can be explained using beam theory and plate buckling theory. The behavior after the peak, however, is quite complex, but is not of interest from a practical standpoint, and will not be discussed.

Web contribution to flexure. The distribution of the longitudinal strains acting on a section through the middle of Fold 8 in Girder G7A, located in a region of significant bending moment near the load point, is given in Figure 21. The longitudinal strains are middle surface strains calculated as an average of the strain gage readings from both sides of the web plate. Figure 21 shows that, regardless of the load level, the web longitudinal strains are very small except for the region close to the flanges. Therefore, the contribution of the web to bending can be reasonably neglected, and, thus, the only significant web stresses are shear stresses, which can be approximated as:

$$\tau = \frac{V}{h_w \, t_w} \tag{8}$$

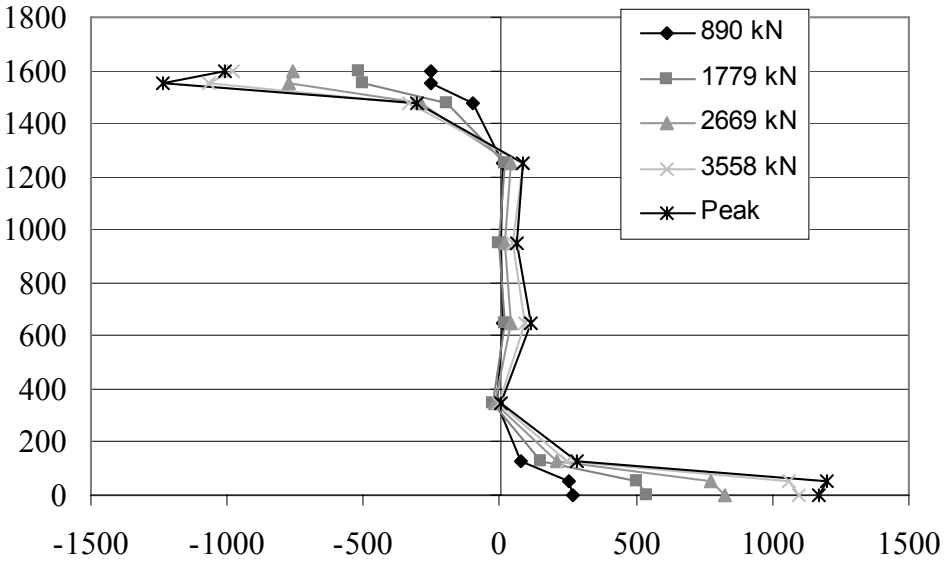

Figure 21. Longitudinal strains over girder depth at Fold 8 of Girder G7A.

Initial stiffness. The initial stiffness of the test specimens can be quantified from the expression $P = k_0 \Delta$, where P is the applied load, k_0 is the initial stiffness, and Δ is the load point deflection. Including both flexure and shear deformations, k_0 is given by:

$$k_0 = \frac{k_b\, k_s}{k_b + k_s} \tag{9}$$

where, k_b (the bending stiffness), and k_s (the shear stiffness) are given by:

$$k_b = \frac{3LEI}{a^2(L-a)^2}$$
$$k_s = \frac{L h_w t_w G}{a(L-a)} \cdot \left(\frac{\beta + \cos\alpha}{\beta + 1} \right) \tag{10}$$

where E and G are the elastic and shear moduli, respectively; a and L are the shear span and overall span, respectively; and I is the moment of inertia of the section for overall girder bending, neglecting the web contribution. The factor in the parentheses involving α and β in the expression for k_s takes into account the reduced stiffness in shear for a corrugated web. This factor will always be less than 1 and should be included in the stiffness calculations. Using the measured specimen dimensions, k_0 is graphically represented in Figures 17 and 18 for Girders G7A and G8A, respectively. The figures show good agreement between the calculated stiffness and the experimental results.

Effect of Imperfections. Measurements of web initial imperfections at the center of the longitudinal folds within the failure shear span (Folds 1 through 9) showed that the web

folds were bent primarily in single curvature with the center of curvature toward the near side of the girder (see Figures 10 and 11). The maximum measured amplitude on Fold 9 of Girder G7A and on Fold 2 of Girder G8A was 4.06mm (0.160in, 64% of t_w) and 5.72mm (0.225in, 91% of t_w), respectively. Fold 9 for Girder G7A and Fold 2 for Girder G8A are believed to have triggered shear failure during the tests. This was evidenced by the measured growth of web out-of-plane deflections during the test.

Revisiting Figure 8, it is seen that the experimental results follow the trend (*i.e.*, decreasing shear capacity with increasing imperfection amplitude) but are slightly higher than the finite element results. The difference is partially attributed to the fact that the imperfection shapes (from the eigenvalue analysis) used in the FE analysis are likely to be more critical than the actual web out-of-flatness geometric imperfections.

To assess the proposed nominal shear strength equations, the results for Girders G7A and G8A are plotted in Figure 3. Equation 7 predicts 70.7% of the shear yield capacity (i.e., $\tau_n / \tau_y = 0.707$), which is much less than the experimental test results. Nevertheless, due to uncertainty in the magnitude and distribution of initial imperfections, the actual shear strength cannot be determined with great confidence and variation in strength is expected. It is therefore recommended that Equation 7 be used in its current form until better methods to predict the shear strength are developed.

4. Flexural Strength of Corrugated Web Girders

The flexural strength of corrugated web girders is a function of the web depth, flange dimensions, and material properties. As noted previously and observed in the results from the shear strength tests (Figure 21), the bending moment is carried almost entirely by the flanges. This section discusses the flexural strength of corrugated web girders. First, the flexural strength of corrugated web girders is considered without concern for the influence of vertical shear force. Then, the influence of shear force is considered.

4.1. Flexural Strength

The flexural strength of corrugated web girders under constant bending moment (without vertical shear force) has been investigated by previous research. This section briefly reviews this research. Ultimate strength, compression flange local buckling, and lateral torsional buckling are addressed.

Ultimate Bending Strength. Elgaaly *et al.* (1997) reported the results of six flexural strength tests of corrugated web girders under 4-point loading. Only the constant moment region between the two loads was corrugated. Four specimens had a corrugated web thickness of 0.61mm (0.024in), and two specimens had a corrugated web thickness of 0.76mm (0.030in). The corresponding web depth-to-thickness ratios were approximately 500 and 400. Different trapezoidal web geometries were used. The angle of corrugation, ranged from 45° to 62.5°. The longitudinal fold width ranged from 19.8mm (0.78in) to 49.8mm (1.96in). The corrugation depth ranged from 14.2mm (0.56in) to 50.8mm

(2.00in). The flange yield strength was taken as 293MPa (42.5ksi) for the first four specimens and 376MPa (54.5ksi) for the second two specimens. All specimens, except for one, failed suddenly due to yielding of the compression flange followed by vertical buckling of the flange into the web. The experimentally determined failure moment, M_{test}, was found to agree with the calculated yield moment, M_{yf}, neglecting the web contribution. The average ratio of M_{test} to M_{yf} was very close to 1.00. Additionally, Elgaaly *et al*. (1997) developed and used finite element models to conduct a parametric study. The parameters included the corrugation profile, the ratio of the web and flange yield stress, and the ratio of the web and flange thicknesses. Elgaaly *et al.* (1997) concluded that the contribution of the web to the ultimate moment capacity of a corrugated web beam is negligible, and that the stresses in the web due to bending are equal to zero except for very close to the flanges where the web is restrained.

Compression Flange Local Buckling. Johnson and Cafolla (1997) conducted a study to determine the flange slenderness (width-to-thickness) ratio to use in calculating the flange local buckling capacity of an I-girder with trapezoidal web corrugations. Using the largest flange overhang, $(b_f + h_r)/2$, where b_f is the flange width and h_r is the corrugation depth, to calculate the flange slenderness is conservative. However, Johnson and Cafolla (1997) found that, within the range of parameters considered in their study, the average flange overhang, $b_f/2$, could be used. Johnson and Cafolla (1997) conducted five tests. The results of these tests were re-evaluated as part of the present study, and compared with the following equation for the flange inelastic local buckling stress, F_{fb}:

$$F_{fb} = F_{yf}\left[1.0 - 0.88\left(\lambda_f\sqrt{\frac{F_{yf}}{\mathrm{E}}} - 0.38\right)\right] \le F_{yf} \tag{11}$$

where F_{yf} is the flange yield stress and λ_f is the flange slenderness ratio. The comparison shows that using $(b_f + h_r)/2t_f$, where t_f is the flange thickness, as the flange slenderness ratio, λ_f, is too conservative, and using $b_f/2t_f$ is potentially unconservative. The comparison shows that using a flange slenderness ratio of $\lambda_f = (b_f + h_r/2)/2t_f$ provides accurate and slightly conservative results for the flange inelastic local buckling stress, F_{fb}.

Lateral Torsional Buckling. Lindner and Aschinger (1990) and Lindner (1990) found that the torsional stiffness of girders with corrugated webs is higher than that of flat web I-girders due to the web corrugations. This increased torsional resistance should lead to an increased *elastic* lateral-torsional buckling capacity. However, the likelihood of a non-uniform normal stress distribution across the flange width (due to flange transverse bending, as discussed below), and the fact that, for bridge I-girders, *inelastic* rather than *elastic* lateral torsional buckling is more likely to control the flexural resistance, suggest that the increased torsional stiffness may not lead to an increased lateral torsional buckling capacity. Until research demonstrates that corrugated web girders have an increased inelastic lateral-torsional buckling resistance, compared to flat web I-girders, the increased torsional stiffness should not be considered in calculating the lateral torsional buckling resistance of corrugated web girders. Thus, the existing lateral

torsional buckling equations for flat web girders are recommended for corrugated web girders, without considering the increased torsional stiffness of corrugated web girders.

4.2. Strength under Combined Flexure and Shear

This section addresses the influence of vertical shear forces on the flexural strength of corrugated web girders. A study reported by Abbas (2003) shows that, owing to the eccentricity of the web, vertical shear forces acting on I-shaped girders with corrugated webs result in transverse bending of the flanges. This section summarizes the results of this study, and presents a simplified approach for considering the effect of this flange transverse bending on the flexural strength of corrugated web bridge girders.

Figure 22 shows the internal forces acting on an infinitesimal segment *dz* of a corrugated web girder. The figure shows three free bodies of length *dz*, namely the top flange, the web, and the bottom flange. N, M_t, V_t, and V_b are internal forces acting on the flanges, and H_x and H_z are internal forces transferred between the web and flanges. V_y is the vertical shear force carried by the web. The variable e defines the eccentricity of the corrugated web with respect to the longitudinal axis (centerline) of the flanges, z. The web eccentricity is a simple function of z, $e(z)$, for a sinusoidal web (*i.e.*, the sine function), and is a piecewise continuous function for a trapezoidal web (*e.g.*, e equals half the corrugation depth, $h_r/2$, along the longitudinal folds of a trapezoidal web). N and V_b are flange forces that develop when overall girder bending moment and vertical shear force act on a corrugated web girder, but flange transverse bending does not occur. Therefore, the following discussion focuses on M_t and V_t, which are the flange transverse bending moment and associated shear that develop due to the eccentricity of the web. M_t and V_t are related as follows:

$$V_t = \frac{dM_t}{dz} \tag{12}$$

From the free body diagrams in Figure 22, a relationship between the flange shear, V_t, and the vertical shear, V_y, can be derived (Abbas 2003):

$$V_t = \frac{-2V_y\, e}{h} + A_1 \tag{13}$$

where, e is the eccentricity of the web given as a function of the position z along the girder length, h is the distance between the middle surfaces of the flanges (which is approximately the web depth, h_w) and A_1 is a constant of integration. V_t and V_y are also functions of position z. Equations 12 and 13 are the starting point for analyzing flange transverse bending in corrugated web I-girders.

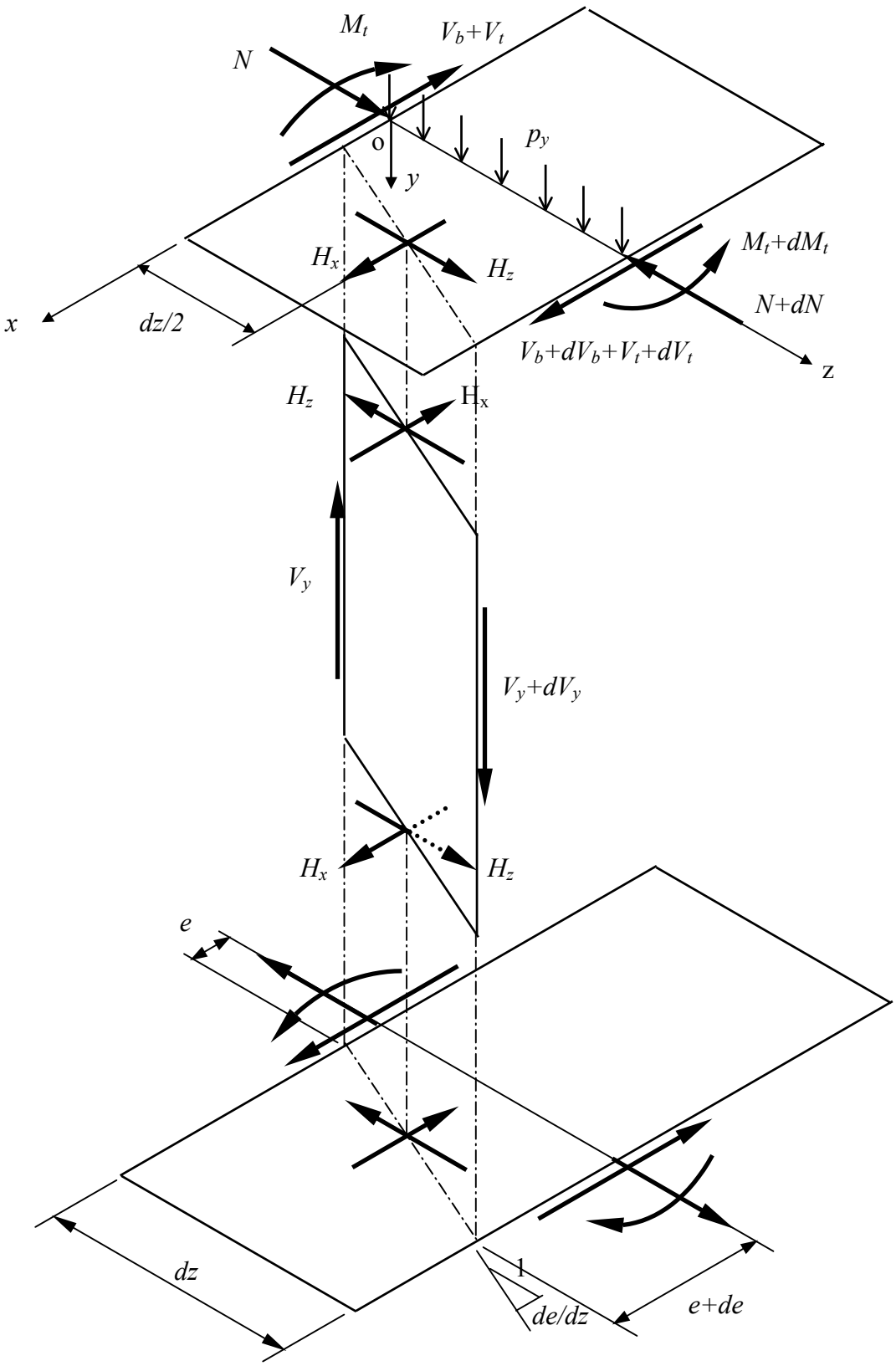

Figure 22. Free body diagrams of corrugated web I-girder components.

Equation 12 suggests that each flange can be analyzed as a beam loaded in its own plane to determine the flange transverse bending moment and deflection. Abbas (2003) introduces two methods for this analysis: (1) direct integration of Equation 13, considering both the loading and boundary conditions, and (2) a fictitious load approach. Only this second, more practical method will be summarized here.

The load used in the fictitious load approach is a transverse load, that if applied to the flange, will produce the same internal flange forces, M_t and V_t, and flange transverse deflection as observed in a corrugated web girder under vertical load. The fictitious load, p_t, is as follows:

$$p_t = -\frac{dV_t}{dz} \tag{14}$$

From Equation 13 and assuming h is constant along the girder length, it follows that:

$$p_t = \frac{2}{h}\left\{V_y \frac{de}{dz} + e\frac{dV_y}{dz}\right\} \tag{15}$$

The term de/dz is related to the slope of the corrugated web relative to the longitudinal axis of the girder, η, as follows:

$$\frac{de}{dz} = \tan\eta \tag{16}$$

For a trapezoidal web, η equals α along the inclined folds and η equals zero along the longitudinal folds. For a sinusoidal web, de/dz is a continuous function of position along the length of the girder, z (*i.e.*, if $e(z)$ is a sine function, de/dz is a cosine function).

The second term in Equation 15 involves the corrugation eccentricity, e, and the change in the vertical shear due to an applied vertical load. Abbas (2003) considered several different vertical load cases. Here, two vertical load cases are considered, the case of a uniform distributed load, p_y, and the case of no distributed load ($p_y = 0$) which produces constant shear, V_y. In either case:

$$\frac{dV_y}{dz} = -p_y \tag{17}$$

and Equation 15 for the fictitious load becomes:

$$p_t = \frac{2}{h}\left\{V_y \tan\eta - ep_y\right\} \tag{18}$$

Equation 18 indicates that the fictitious transverse load in a region of constant vertical shear ($p_y = 0$) is directly related to the corrugation slope η. Hence, for a trapezoidal web,

p_t is either zero for longitudinal folds (since *tan* η is zero) or uniform over the inclined folds (since *tan* η is a constant equal to *tan* α). Figure 23a shows the fictitious load for a trapezoidal web with constant vertical shear. Similarly, the fictitious load for a trapezoidal web under the case of uniform vertical load, p_y, is shown in Figure 23b. Although, the fictitious load pattern is slightly more complicated than that shown in Figure 23a, the fictitious load is either uniform, or linearly varying.

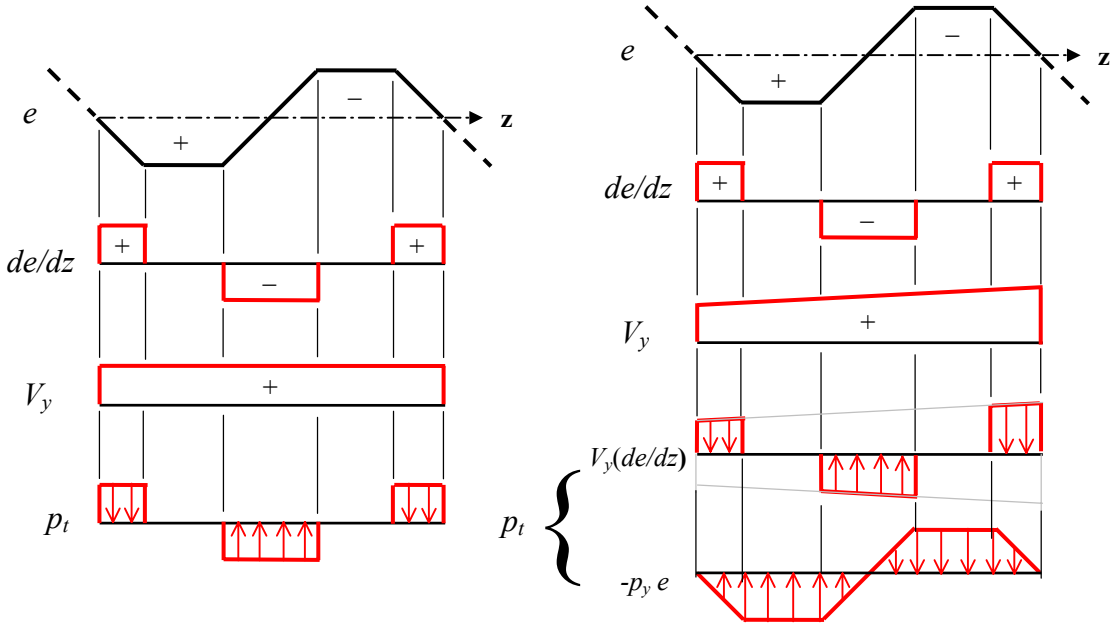

(a) Trapezoidal web with constant vertical shear

(b) Trapezoidal web with linearly varying vertical shear due to a uniform distributed load p_y

Figure 23. Fictitious load patterns.

The flange transverse bending moment and deflection can be determined from the fictitious loads using structural analysis. Abbas (2003) presents results for both trapezoidal and sinusoidal corrugated web girders under several loading and boundary conditions. Figures 24 and 25 show results for a simply supported girder under a uniform distributed load (Abbas 2003). The span of the girder, L, is equal to n times the corrugation wave length. It is assumed that the girder is braced laterally only at each end of the span, and that each end is supported so each reaction is located at the center of an inclined fold. As noted earlier, p_y is the uniform distributed load and h is the distance between the flange middle surfaces. e_0 is the amplitude of the corrugation eccentricity, e, which equals half the corrugation depth, $h_r/2$. The results show that the amplitude of the flange transverse bending moment tends to decrease with a decrease in the corrugation wave length (as n increases), and that the flange transverse bending moment is larger for a girder with trapezoidal corrugations. Also, the results differ significantly when the girder web is composed of an odd number of half corrugation waves compared to the results for an even number of half corrugation waves (*i.e.*, when the girder span is a whole multiple of the corrugation wave length). Note that when each reaction is located at the center of an inclined fold, n must equal a whole number multiple of 1/2 (*i.e.*, 1/2, 2/2, 3/2, *etc*.).

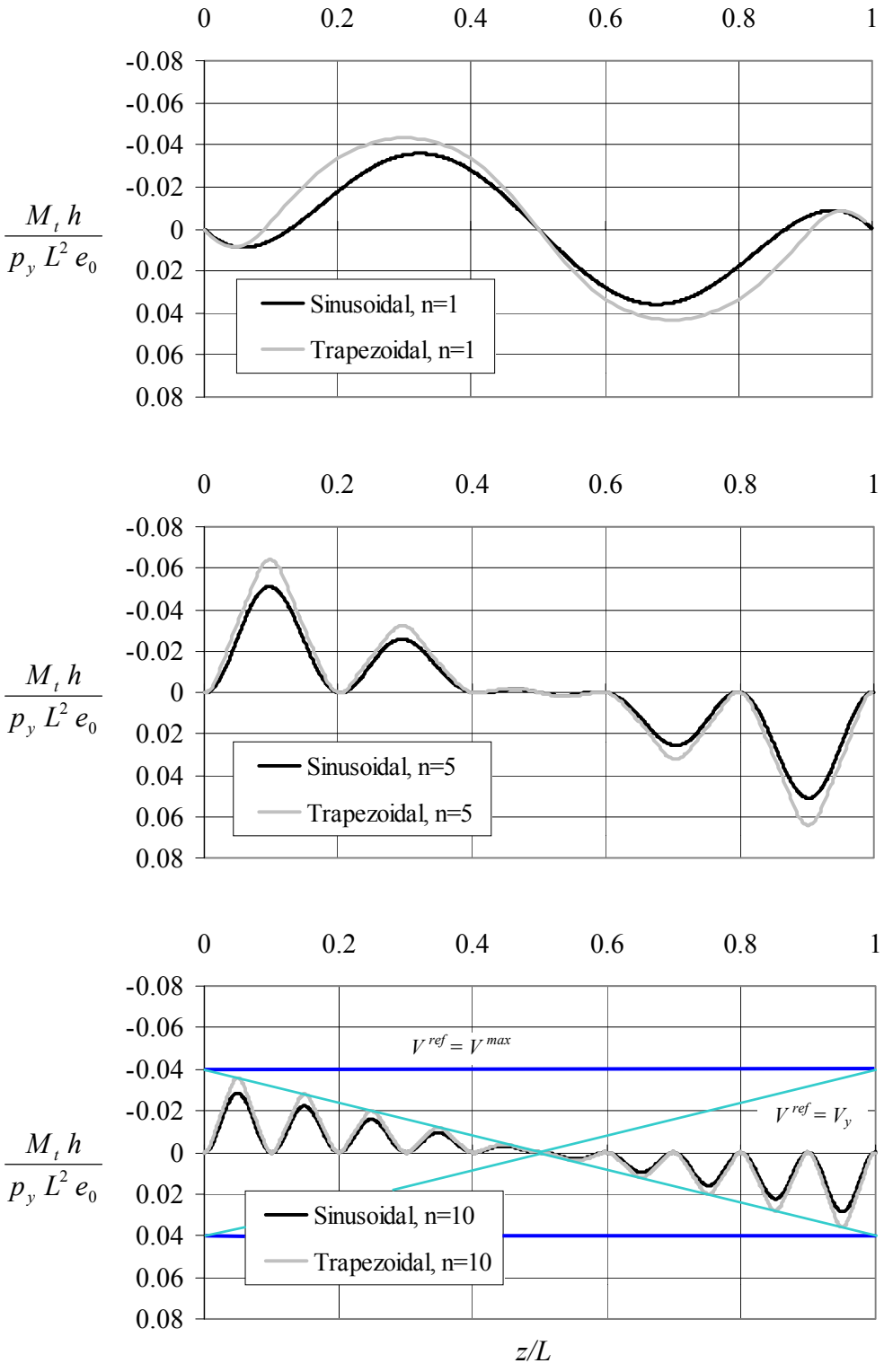

Figure 24. Flange transverse bending for even number of half corrugations.

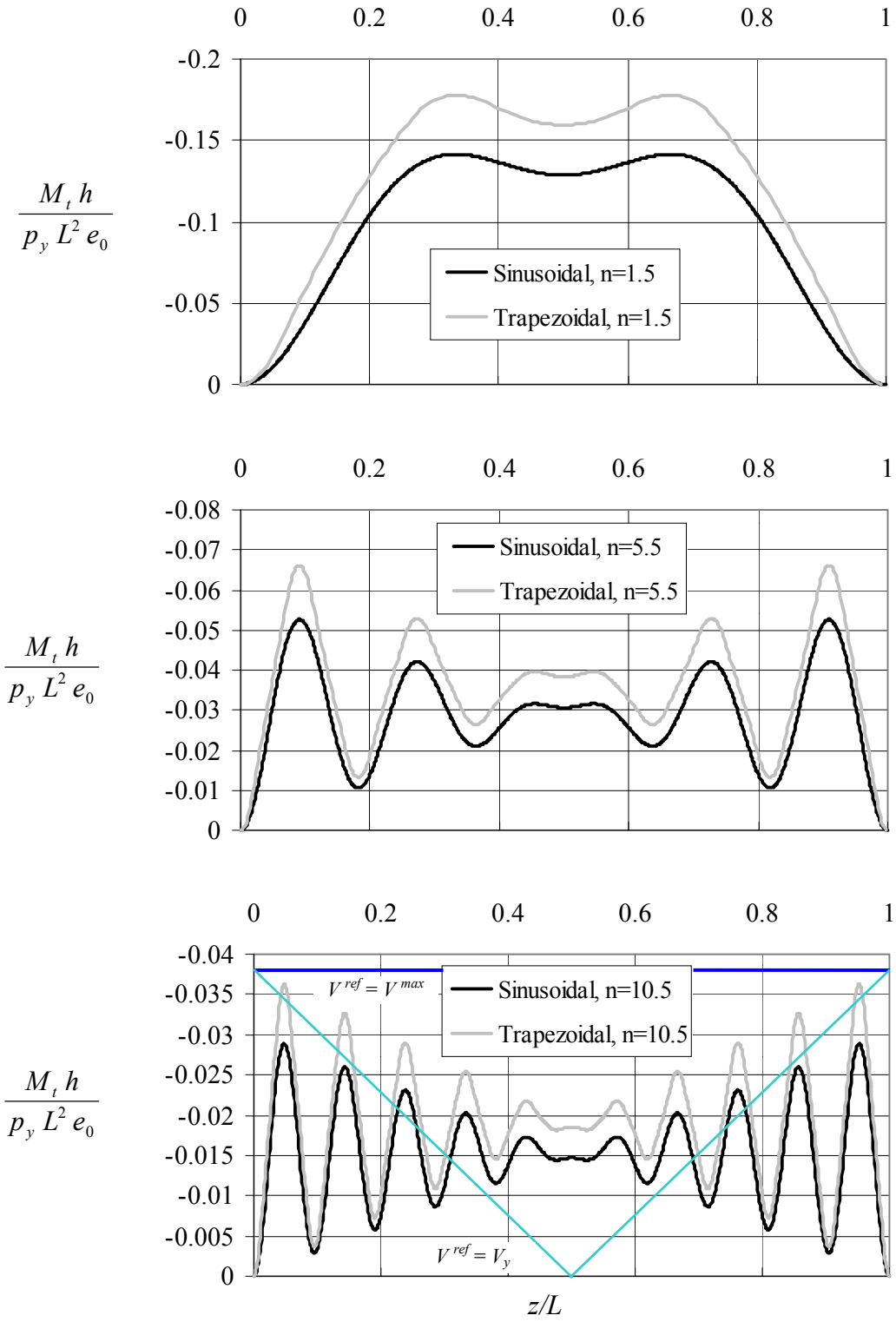

Figure 25. Flange transverse bending for odd number of half corrugations.

Thus, the variation of flange transverse bending moment, M_t, along the length of a corrugated web I-girder can be determined by theoretical analysis. Abbas (2003) validated these analytical results using results from FE analysis, and experimental results. However, the analysis methods outlined above are, in many cases, too involved for the design of corrugated web bridge girders. Therefore, the following simpler expression for M_t is suggested:

$$M_t = \frac{2V^{ref}}{h} A_0 \tag{19}$$

where, V^{ref} is the reference vertical shear used to calculate M_t at a given cross-section of the girder (as discussed below), and A_0 is the area under one half corrugation wave. For a trapezoidal web, A_0 equals (b+d/2) h_r/2 (which equals (b+d/2) e_0), where b, d, and h_r are as shown in Figure 1.

Note that at every section within a bridge girder span, M_t, from Equation 19, should be combined with other load effects in the flange, such as overall girder bending stresses and wind load effects, to determine if the girder flange satisfies the applicable design specifications, such as the AASHTO bridge design specifications (AASHTO 1998). A discussion of how to include M_t in the design of bridge girders is given in Section 6 of this report. Here, only the reference shear, V^{ref}, to be used to calculate M_t at each section of a bridge girder, is considered.

Abbas (2003) suggests using the maximum vertical shear within the span (*i.e.*, the maximum value of V_y), V^{max}, as V^{ref}. This is a simple, but perhaps overly conservative approach. The horizontal lines in Figures 24 and 25 (labeled $V^{ref} = V^{max}$) compare M_t from Equation 19, using $V^{ref} = V^{max}$, with the previous M_t results for a simply supported girder with a trapezoidal web under uniform distributed load when n equal 10 and 10.5 respectively. The comparison shows that using $V^{ref} = V^{max}$ in Equation 19, although simple, is overly conservative near midspan where V_y is close to zero. Another simple approach is to use the concurrent vertical shear, V_y, at each section to calculate M_t at that section (*i.e.*, use $V^{ref} = V_y$). The inclined lines in Figures 24 and 25 (labeled $V^{ref} = V_y$) compare M_t from Equation 19, using $V^{ref} = V_y$, with the previous M_t results. The comparison shows that Equation 19 with $V^{ref} = V_y$ provides a close bound to the previous results for n equal 10, but is unconservative for n equal 10.5.

It should be pointed out that the results presented in Figures 24 and 25 are for a girder braced only at the ends of the span. Corrugated web bridge girders are expected to be braced, at a minimum, by a few interior cross frames, and it can be shown by analysis that a few (one or two) braces within the span will significantly reduce M_t for cases similar to those shown in Figure 25, where M_t is large in the midspan region although V_y is relatively small in this region.

However, it is possible to generate combinations of loading conditions and boundary conditions other than those shown in Figure 25, where Equation 19 with $V^{ref} = V_y$ provides unconservative results. In particular, M_t results from rigorous analysis of cases

with concentrated loads will often exceed M_t from Equation 19, using $V^{ref} = V_y$. This unconservative result will occur when the concentrated load is near one end of the span, and, as a result, V_y may be quite small for much of the span. However, the large concentrated loads considered in girder bridge design are almost always moving loads, and, thus, the girders are designed for a shear envelope, V^{env}. It can be shown that calculating M_t from Equation 19, using $V^{ref} = V^{env}$ will generally provide conservative results for concentrated load cases.

In summary, Equation 19 can be used to calculate the flange transverse bending moment due to vertical shear forces acting on corrugated web girders, M_t. Using this equation, M_t should be calculated at every cross section within a bridge girder span and combined with other load effects in the flange. V^{ref} is the shear at each cross section that should be used to calculate M_t. V^{ref} can be conservatively taken as the maximum vertical shear within the span, V^{max} (*i.e.*, the maximum value of V_y), but this is perhaps overly conservative. A more reasonable recommendation is to use $V^{ref} = V^{env}$, the shear envelope value at the cross section, with a lower limit on V^{ref} of $0.25V^{max}$ for cross sections where V^{env} is particularly low. This approach is applicable when: (1) each reaction is located at the center of an inclined fold, and, thus, the girder span is n times the corrugation wave length with n being a whole number multiple of 1/2 (*i.e.*, 1/2, 2/2, 3/2, *etc*.), and (2) at least one interior cross-frame is provided within the span.

5. Preliminary Design Study of Corrugated Web Bridge Girders

A preliminary design study of corrugated web bridge girders was conducted. The study compares the weight of corrugated web girders with the weight of conventional flat web I-girders. Factors other than weight, including changes in fabrication methods, new fabrication processes, and fabrication equipment investments were not considered due to the lack of information on these factors at the time of the study. The weight of stiffeners and cross frames (or diaphragms) was not included in the comparison.

The preliminary design study was performed at the beginning of the project, and, therefore, the study does not consider the design criteria for corrugated web girders developed by other tasks of Work Area 1. Rather, the study was based on information in publications available at the beginning of the project (*e.g.*, Elgaaly *et al.* 1996; and Elgaaly *et al.* 1997). The work described in Sections 2, 3, and 4 of this report has produced more conservative recommendations for shear and flexural strength, and the use of these more conservative recommendations would change the specific results of the preliminary design study. These impacts have been estimated and are discussed in Section 5.4. Most importantly, however, the preliminary design study results enabled the project to select a web corrugation geometry at the beginning of the project, which has been used throughout other work areas of the project.

5.1. Design Parameters

Only simple span bridges were studied. The webs and flanges of the girders were assumed to be ASTM A709, grade HPS-485W steel (ASTM 2001). The following span length, girder spacing, and web depth parameter values were considered in the study:

span length: 40m (131ft), 50 m (164ft).
girder spacing: 3600mm (11.8ft), 4600mm (15.0ft).
web depth: 1500mm (59.1in), 1800mm (70.9in), 2100mm (82.7in) for 40m span.
1800mm (70.9in), 2100mm (82.7in), 2400mm (94.5in) for 50m span.

The bridges were assumed to have no skew. For each girder design, the web thickness was kept constant and only one transition in the flange size was assumed in the design. The study considered only the interior girders of each bridge.

Twelve different combinations of span length, girder spacing and web depth were studied. The twelve cases are identified using notation to identify the value of each of the three parameters. Each case is designated as: Lxx-yy-z, where:

xx is the girder length in meters,
yy is 1/100 of the web depth in millimeters,
z is "n" for the narrow girder spacing, *i.e*, 3600mm (11.8ft),
"w" for the wide girder spacing, *i.e*, 4600mm (15.0ft).

For example, the case designated L40-15-n refers to the case with 40m (131ft) span length, 1500mm (59.1in) web depth, and narrow (3600mm (11.8ft)) girder spacing.

5.2. Flat Web I-Girders

A conventional flat web I-girder was designed for each case of span length, girder spacing, and web depth using the design program STLRFD. This program was developed by PennDOT to design steel girders according to the AASHTO LRFD bridge design specifications (AASHTO 1998). The program is based on a line-girder approach that utilizes the live load distribution factors from the AASHTO LRFD specifications. Other loads, such as the structural component weight and the weight of a wearing surface, were applied in accordance to the specifications. Minimum flange plate dimensions and web thickness were determined based on the current PennDOT practices.

Table 3 lists the web and flange dimensions for the twelve cases. Two rows are shown for each case. The first row shows the dimensions in the end section of the girder, that is, from the end of the girder to the transition in the flange. The second row shows the dimensions in the middle section of the girder. For each case, the second column of the table shows the distance from the end of the girder to the location of the flange transition. Notice that in some cases, there were no transitions in the flange. In these cases, the dimensions of the flanges along the full length of the girders are controlled by the

minimum flange plate dimensions. These minimum dimensions are controlled by the minimum flange thickness, taken as 20mm (13/16in), and the minimum width needed to accommodate the required shear connectors.

Table 3. Flat web I-girder dimensions.

Case Designation	Transition Location (from end) (m)	Web Depth (mm)	Web Thickness (mm)	Top Flange Width (mm)	Top Flange Thickness (mm)	Bottom Flange Width (mm)	Bottom Flange Thickness (mm)	Weight per Girder (kg)
L40-15-n	6.68	1500	16	400	25	400	32	5209
		1500	16	400	25	400	60	
L40-18-n	*	1800	16	400	20	550	32	5222
		1800	16	400	20	550	32	
L40-21-n	*	2100	16	400	25	500	25	5386
		2100	16	400	25	500	25	
L50-18-n	8.35	1800	16	450	32	500	32	8223
		1800	16	450	32	500	60	
L50-21-n	8.35	2100	18	450	25	450	25	8135
		2100	18	450	25	450	50	
L50-24-n	8.35	2400	18	350	25	350	25	8543
		2400	18	350	45	350	50	
L40-15-w	6.68	1500	18	450	25	550	32	6170
		1500	18	450	25	550	55	
L40-18-w	6.68	1800	16	400	32	400	32	5938
		1800	16	400	32	400	60	
L40-21-w	*	2100	18	400	25	550	32	6278
		2100	18	400	25	550	32	
L50-18-w	8.35	1800	18	550	32	550	38	9915
		1800	18	550	32	550	70	
L50-21-w	8.35	2100	18	500	32	500	32	9495
		2100	18	500	32	500	60	
L50-24-w	8.35	2400	20	500	25	550	25	9789
		2400	20	500	25	550	45	

* no transition.

5.3. Corrugated Web Girders with Trapezoidal Corrugations

Corrugated web girders with trapezoidal corrugations were designed for each case of span length, girder spacing, and web depth. The eight different corrugation shapes shown in Figure 26 were considered in the design study, so that for each case of span length, girder spacing, and web depth, eight different girders were designed.

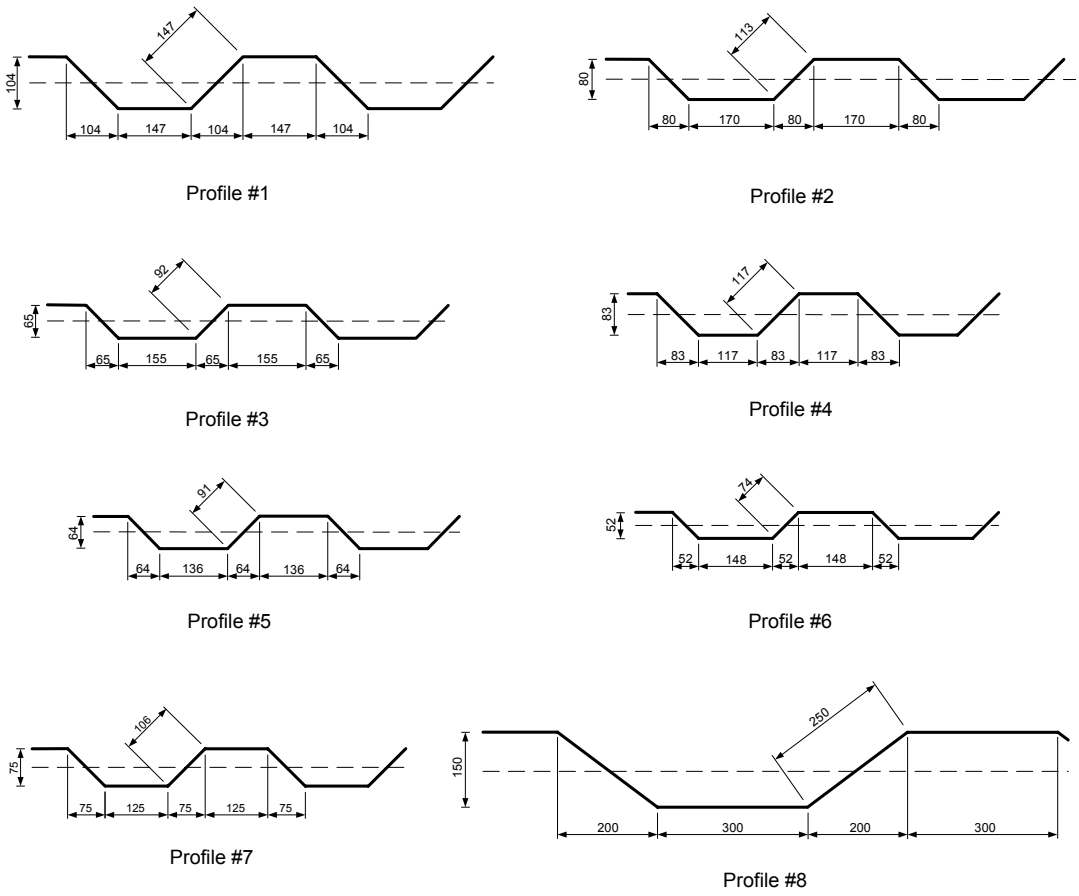

Figure 26. Corrugation geometries (dimensions in mm).

The corrugated webs were assumed to resist the shear forces while the flanges were assumed to resist the bending moment. Spreadsheet programs were used to determine the flange dimensions and the web thickness required for the girders with corrugated webs.

For each case in the study, the required flange dimensions were determined using a trial and error approach. The widths of the top and bottom flanges were assumed to be equal to the widths of the flanges of the corresponding conventional flat web I-girder. A flange transition was assumed to be present at the same location as in the corresponding flat web I-girder. The thickness of each flange was assumed and the moment of inertia and section modulus were calculated assuming the web does not contribute to the flexural stiffness and strength. The section modulus was calculated for the non-composite steel section, the short-term composite section, and the long-term composite section (AASHTO 1998). The flange stresses were calculated using the appropriate section modulus, and if the stresses were too large, the flange thickness was increased.

Since the preliminary design study was conducted early in the project, before the results described in Section 5 were available, the stresses in the flanges were calculated

neglecting flange transverse bending and considering only overall girder bending stresses. Bending stresses from the weight of the girders and deck were calculated using the properties of the non-composite steel section. The stresses from live loads and from superimposed dead loads (e.g., a wearing surface) were calculated using the section properties of the short-term and long-term composite sections, respectively. The assumed thickness of each of the flanges was increased until the flange stresses calculated for the corrugated web girders were comparable to those calculated for the corresponding conventional plate girder. Table 4 lists the required flange dimensions. Since the corrugated web does not contribute significantly to the flexural resistance, the flange dimensions in Table 4 are applicable to all the corrugated web shapes considered in the study, regardless of the corrugation geometry or web thickness.

Table 4. Flange dimensions for corrugated web girders.

Designation	Transition Location (from end) (m)	Top Flange Width (mm)	Top Flange Thickness (mm)	Bottom Flange Width (mm)	Bottom Flange Thickness (mm)
L40-15-n	6.68	400	28	400	45
		400	35	400	70
L40-18-n	*	400	28	550	40
		400	28	550	40
L40-21-n	*	400	32	500	38
		400	32	500	38
L50-18-n	8.35	450	35	500	45
		450	40	500	70
L50-21-n	8.35	450	32	450	45
		450	35	450	70
L50-24-n	8.35	350	38	350	55
		350	60	350	80
L40-15-w	6.68	450	35	550	45
		450	38	550	60
L40-18-w	6.68	400	38	400	50
		400	40	400	80
L40-21-w	*	400	38	550	45
		400	38	550	45
L50-18-w	8.35	550	40	550	50
		550	40	550	80
L50-21-w	8.35	500	38	500	50
		500	45	500	70
L50-24-w	8.35	500	32	550	45
		500	38	550	60

* no transition.

The nominal shear strength of the corrugated webs was determined in accordance with the recommendations of Elgaaly *et al.* (1996) considering three possible shear failure modes: (1) local buckling, with shear strength given by Equation 1 with k_L = 7.16; (2) global buckling, with shear strength given by Equation 2 with k_G = 32.4; and (3) shear yield, with the shear strength given by Equation 6. In considering these three failure modes, shear yield was used as the upper bound shear strength, which controlled most of the designs. As discussed below, in a few cases, the buckling strength was lower and controlled the designs.

As noted above, the preliminary design study was conducted early in the project, using results available at the time. Thus the values of k_L and k_G are not as conservative as those used in Section 2.2, and Equations 5 and 7 were not used. As discussed in Section 5.4, some of the web thickness results in this preliminary design study need to be increased to provide sufficient shear strength when the shear strength is based on Equations 5 and 7.

The corrugated web girder designs were made considering the following web thickness limits: (1) no web thickness limit; (2) a minimum web thickness of 6mm (1/4in); and (3) a minimum web thickness of 9mm (11/32in).

Table 5 lists the required web thickness for the eight corrugation geometries shown in Figure 26 for each of the twelve cases of span length, girder spacing, and web depth. The results in the table are developed for the case with no minimum web thickness limit. The table also lists the ratio of the weight of the corrugated web girders to the weight of the least-weight flat web I-girder. In each case, the least-weight flat web I-girder is the lightest flat web I-girder designed for the same span length and girder spacing as the corrugated web girder, but may have a different web depth.

Notice that for most cases, the nominal shear strength was controlled by shear yield (Equation 6) rather than by buckling. The exceptions are the 2400mm (94.5in) deep webs for Profiles #3 and #5 and the 2100mm (82.7in) and 2400mm (94.5in) deep webs for Profile #6. For most of the cases controlled by global buckling, the nominal shear strength was close to the shear yield strength, so that being controlled by global buckling (rather than shear yield) did not increase the required web thickness. Among the cases controlled by global buckling, only for the cases with the 2400mm (94.5in) deep web for Profile #6 did the difference between the global buckling strength and shear yield strength result in an increase in the required web thickness.

Tables 6 and 7 are similar to Table 5 except that results are based on a minimum web thickness of 6mm (1/4in) and 9mm (11/32in), respectively. For the 6mm (1/4in) minimum web thickness cases shown in Table 6, all webs have the minimum (6mm) thickness except for the L-40-15-w and L-50-18-w cases which required 7mm (9/32in) thick webs for all profiles, as shown in Table 6. For the 9mm (11/32in) minimum web thickness cases shown in Table 9, all webs have the minimum (9mm) thickness. Since the same web thickness is used for all the corrugation geometries, the difference in weight ratios in Table 9 is a function of the ratio between the length of the web along the corrugations and the projection of the web corrugations along the centerline of the girder.

Table 5. Web thickness of trapezoidal web girders and weight comparison to flat web I-girders - no web thickness limit.

Designation	Transition Location (from end) (m)	Web Depth (mm)	Profile #1		Profile #2		Profile #3		Profile #4		Profile #5		Profile #6		Profile #7		Profile #8	
			tw (mm)	Weight Ratio	tw (mm)	Weight Ratio	tw (mm)	Weight Ratio	tw (mm)	Weight Ratio	tw (mm)	Weight Ratio	tw (mm)	Weight Ratio	tw (mm)	Weight Ratio	tw (mm)	Weight Ratio
L40-15-n	6.68	1500	5.5	0.873	5.5	0.868	5.5	0.866	5.5	0.873	5.5	0.868	5.5	0.864	5.5	0.871	5.5	0.863
		1500	5.5		5.5		5.5		5.5		5.5		5.5		5.5		5.5	
L40-18-n	*	1800	5	0.806	5	0.800	5	0.798	5	0.806	5	0.800	5	0.795	5	0.803	5	0.794
		1800	5		5		5		5		5		5		5		5	
L40-21-n	*	2100	4	0.767	4	0.761	4	0.760	4	0.767	4	0.761	5	0.800	4	0.765	4	0.756
		2100	4		4		4		4		4		5		4		4	
L50-18-n	8.35	1800	5.5	0.880	5.5	0.875	5.5	0.873	5.5	0.880	5.5	0.875	5.5	0.871	5.5	0.878	5.5	0.870
		1800	5.5		5.5		5.5		5.5		5.5		5.5		5.5		5.5	
L50-21-n	8.35	2100	5	0.816	5	0.810	5	0.809	5	0.816	5	0.810	5	0.806	5	0.814	5	0.805
		2100	5		5		5		5		5		5		5		5	
L50-24-n	8.35	2400	5	0.849	5	0.842	5	0.840	5	0.849	5	0.842	5	0.838	5	0.846	5	0.836
		2400	5		5		5		5		5		5		5		5	
L40-15-w	6.68	1500	7	0.957	7	0.950	7	0.949	7	0.957	7	0.950	7	0.946	7	0.954	7	0.945
		1500	7		7		7		7		7		7		7		7	
L40-18-w	6.68	1800	6	0.911	6	0.905	6	0.903	6	0.911	6	0.905	6	0.900	6	0.908	6	0.899
		1800	6		6		6		6		6		6		6		6	
L40-21-w	*	2100	5	0.845	5	0.838	5	0.836	5	0.844	5	0.838	6	0.871	5	0.842	5	0.833
		2100	5		5		5		5		5		6		5		5	
L50-18-w	8.35	1800	7	0.951	7	0.945	7	0.943	7	0.951	7	0.945	7	0.941	7	0.948	7	0.940
		1800	7		7		7		7		7		7		7		7	
L50-21-w	8.35	2100	5.5	0.841	5.5	0.835	5.5	0.834	5.5	0.841	5.5	0.835	6	0.846	5.5	0.838	5.5	0.830
		2100	5.5		5.5		5.5		5.5		5.5		6		5.5		5.5	
L50-24-w	8.35	2400	5	0.787	5	0.782	5.5	0.797	5	0.787	5	0.782	6	0.811	5	0.785	5	0.777
		2400	5		5		5.5		5		5		6		5		5	

* no transition

Table 6. Weight comparison of trapezoidal web girders to flat web I-girders – 6mm minimum web thickness.

Designation	Transition Location (from end) (m)	Web Depth (mm)	Weight Ratio							
			Profile #1	Profile #2	Profile #3	Profile #4	Profile #5	Profile #6	Profile #7	Profile #8
L40-15-n	6.68	1500 1500	0.890	0.883	0.881	0.889	0.883	0.879	0.887	0.878
L40-18-n	*	1800 1800	0.845	0.837	0.835	0.845	0.837	0.832	0.842	0.831
L40-21-n	*	2100 2100	0.858	0.849	0.847	0.858	0.849	0.843	0.854	0.842
L50-18-n	8.35	1800 1800	0.896	0.890	0.888	0.896	0.890	0.885	0.893	0.884
L50-21-n	8.35	2100 2100	0.853	0.845	0.843	0.852	0.845	0.841	0.850	0.839
L50-24-n	8.35	2400 2400	0.891	0.882	0.880	0.890	0.882	0.877	0.887	0.875
L40-15-w	6.68	1500 1500	0.957	0.950	0.949	0.957	0.950	0.946	0.954	0.945
L40-18-w	6.68	1800 1800	0.911	0.905	0.903	0.911	0.905	0.900	0.908	0.899
L40-21-w	*	2100 2100	0.884	0.877	0.874	0.884	0.877	0.871	0.881	0.870
L50-18-w	8.35	1800 1800	0.951	0.945	0.943	0.951	0.945	0.941	0.948	0.940
L50-21-w	8.35	2100 2100	0.856	0.850	0.848	0.856	0.850	0.846	0.854	0.845
L50-24-w	8.35	2400 2400	0.823	0.816	0.814	0.823	0.816	0.811	0.820	0.810

* no transition

Table 7. Weight comparison of trapezoidal web girders to flat web I-girders – 9mm minimum web thickness.

Designation	Transition Location (from end) (m)	Web Depth (mm)	Weight Ratio							
			Profile #1	Profile #2	Profile #3	Profile #4	Profile #5	Profile #6	Profile #7	Profile #8
L40-15-n	6.68	1500 1500	0.987	0.977	0.974	0.986	0.977	0.971	0.983	0.969
L40-18-n	*	1800 1800	0.962	0.950	0.947	0.961	0.950	0.942	0.957	0.940
L40-21-n	*	2100 2100	0.994	0.981	0.977	0.994	0.981	0.972	0.988	0.969
L50-18-n	8.35	1800 1800	0.989	0.980	0.977	0.989	0.980	0.974	0.985	0.972
L50-21-n	8.35	2100 2100	0.961	0.951	0.948	0.961	0.951	0.944	0.957	0.942
L50-24-n	8.35	2400 2400	1.015	1.003	0.999	1.015	1.003	0.994	1.010	0.992
L40-15-w	6.68	1500 1500	1.014	1.005	1.003	1.013	1.005	1.000	1.010	0.998
L40-18-w	6.68	1800 1800	1.014	1.004	1.001	1.013	1.004	0.997	1.009	0.995
L40-21-w	*	2100 2100	1.004	0.992	0.989	1.003	0.992	0.984	0.999	0.982
L50-18-w	8.35	1800 1800	1.004	0.996	0.994	1.004	0.996	0.991	1.001	0.990
L50-21-w	8.35	2100 2100	0.950	0.940	0.938	0.949	0.940	0.934	0.946	0.932
L50-24-w	8.35	2400 2400	0.929	0.919	0.916	0.929	0.919	0.912	0.925	0.910

* no transition.

5.4. Corrugated Web Girders with Sinusodal Corrugations

Corrugated web girders with sinusoidal corrugations were designed for each case of span length, girder spacing, and web depth. The eight different sinusoidal corrugation shapes, corresponding to the trapezoidal corrugation shown in Figure 26, were considered in the design study, so that for each case of span length, girder spacing, and web depth, eight different girders were designed. Each sinusoidal shape was derived from the corresponding trapezoidal shape assuming that the two shapes have the same corrugation depth, h_r, and corrugation wave length. Figure 27 shows a sinusoidal profile and the corresponding trapezoidal profile.

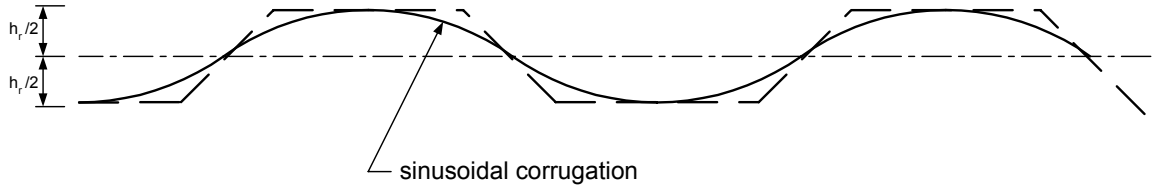

Figure 27. Sinusoidal and corresponding trapezoidal corrugation geometry.

Since the corrugated web does not contribute significantly to the flexural stiffness or strength, the flange dimensions in Table 4 were also used for the girders with sinusoidal web corrugations.

The nominal shear strength of the sinusoidal corrugated webs was based on three shear failure modes: local buckling, global buckling, and shear yield. Except for the parameter D_y, used in Equation 2, the web properties and the local and global buckling shear strengths of the sinusoidal profiles were calculated using the dimensions of the corresponding trapezoidal profiles. The calculation of D_y requires the strong axis moment of inertia of the corrugation geometry to be calculated. For the sinusoidal corrugations, the moment of inertia was calculated by numerical integration. For each integration, the corrugation wave was divided into 200 segments of equal length along the girder longitudinal axis. The actual curved length and the center of gravity of each these segments were determined, and the moment of inertia was calculated as the sum of the moment of inertias of these segments around the longitudinal axis of the girder.

The designs for the girders with sinusoidal web corrugations were made considering the following web thickness limits: (1) no web thickness limit; (2) a minimum web thickness of 6mm (1/4in); and (3) a minimum web thickness of 9mm (11/32in).

Table 8 lists the required web thickness for the eight corrugation geometries for each of the twelve cases of span length, girder spacing, and web depth. The results in the table

are developed for the case with no web thickness limit. The table also lists the ratio of the weight of the corrugated web girders to the weight of the least-weight flat web I-girder.

The use of the sinusoidal corrugations resulted in a reduction in D_y for the girders with sinusoidal corrugations relative to the corresponding girders with trapezoidal corrugations. This reduction in D_y resulted in global buckling controlling a significant number of cases. A comparison of Tables 8 and 5 shows that many of the sinusoidal webs controlled by global buckling required thicker webs than the corresponding trapezoidal webs. However, due to the difference in corrugation shape, the length along the corrugations is shorter for the sinusoidal corrugations than for the corresponding trapezoidal corrugations leading to a reduction of approximately 4% in the web weight when the girder length, web depth and web thickness are the same.

Tables 9 and 10 are similar to Table 8 except that results are based on a minimum web thickness of 6mm (1/4in) and 9mm (11/32in), respectively. For the 6mm (1/4in) minimum web thickness cases shown in Table 9, some webs have the minimum thickness however, many cases require thicker webs (see the web thickness results in Table 8). For the 9mm (11/32in) minimum web thickness cases shown in Table 10, all webs have the minimum thickness except the L-50-24-w case for Profile #6 which requires a web thickness of 10mm (13/32in) (see Table 8).

Notice that Tables 8 through 10 are analagous to Tables 5 through 7. Comparing each pair of tables shows the effect of changing the trapezoidal corrugations to sinusoidal corrugations. The effect of such a change is a small reduction (approximately 1%) in the girder weight when the web thickness does not change. For the cases where the girder web thickness increases, the girder weight, assuming no web thickness limit, increases by up to 14%. The largest increases occurred when a deep web with shallow corrugations was considered. When a minimum web thickness was assumed, the web thickness is more often the same for both the sinusoidal and trapezoidal webs and, consequently, the girders with sinusoidal webs more often have a smaller weight. When a 6mm (1/4in) minimum web thickness was assumed, only 14 out of the 96 cases had a larger weight when a sinusoidal web was used. When a 9mm (11/32in) minimum web thickness was assumed, only one out of the 96 cases had a larger weight when a sinusoidal web was used.

Table 8. Web thickness of sinusoidal web girders and weight comparison to flat web I-girders - no web thickness limit.

Designation	Transition Location (from end) (m)	Web Depth (mm)	Profile #1		Profile #2		Profile #3		Profile #4		Profile #5		Profile #6		Profile #7		Profile #8	
			tw (mm)	Weight Ratio	tw (mm)	Weight Ratio	tw (mm)	Weight Ratio	tw (mm)	Weight Ratio	tw (mm)	Weight Ratio	tw (mm)	Weight Ratio	tw (mm)	Weight Ratio	tw (mm)	Weight Ratio
L40-15-n	6.68	1500	5.5	0.863	5.5	0.856	5.5	0.855	5.5	0.863	5.5	0.856	5.5	0.855	5.5	0.863	5.5	0.855
		1500	5.5		5.5		5.5		5.5		5.5		5.5		5.5		5.5	
L40-18-n	*	1800	5	0.794	5	0.788	5	0.786	5	0.794	5.5	0.805	7	0.856	5	0.794	5	0.786
		1800	5		5		5		5		5.5		7		5		5	
L40-21-n	*	2100	4	0.756	5	0.791	6	0.830	5	0.799	5.5	0.812	7	0.871	5	0.799	4	0.749
		2100	4		5		6		5		5.5		7		5		4	
L50-18-n	8.35	1800	5.5	0.870	5.5	0.864	5.5	0.862	5.5	0.870	5.5	0.864	7	0.904	5.5	0.870	5.5	0.862
		1800	5.5		5.5		5.5		5.5		5.5		7		5.5		5.5	
L50-21-n	8.35	2100	5	0.805	5	0.799	6	0.830	5.5	0.822	6	0.832	8	0.895	6	0.839	5	0.798
		2100	5		5		6		5.5		6		8		6		5	
L50-24-n	8.35	2400	5	0.836	6	0.867	7	0.902	5.5	0.856	7	0.904	8	0.939	6	0.875	5	0.828
		2400	5		6		7		5.5		7		8		6		5	
l40-15-w	6.68	1500	7	0.945	7	0.938	7	0.936	7	0.945	7	0.938	7	0.936	7	0.945	7	0.936
		1500	7		7		7		7		7		7		7		7	
L40-18-w	6.68	1800	6	0.899	6	0.892	7	0.921	6	0.899	7	0.923	7	0.921	6	0.899	6	0.890
		1800	6		6		7		6		7		7		6		6	
L40-21-w	*	2100	5	0.833	5	0.826	7	0.895	5	0.833	7	0.898	8	0.931	6	0.870	5	0.824
		2100	5		5		7		5		7		8		6		5	
L50-18-w	8.35	1800	7	0.940	7	0.933	7	0.932	7	0.940	7	0.933	8	0.956	7	0.940	7	0.932
		1800	7		7		7		7		7		8		7		7	
L50-21-w	8.35	2100	5.5	0.830	5.5	0.824	7	0.865	6	0.845	7	0.867	9	0.921	7	0.874	5.5	0.823
		2100	5.5		5.5		7		6		7		9		7		5.5	
L50-24-w	8.35	2400	5	0.777	6	0.803	8	0.864	6	0.810	8	0.867	10	0.928	7	0.843	5	0.769
		2400	5		6		8		6		8		10		7		5	

* no transition

Table 9. Weight comparison of sinusoidal web girders to flat web I-girders – 6mm minimum web thickness.

Designation	Transition Location (from end) (m)	Web Depth (mm)	Weight Ratio							
			Profile #1	Profile #2	Profile #3	Profile #4	Profile #5	Profile #6	Profile #7	Profile #8
L40-15-n	6.68	1500 1500	0.878	0.871	0.869	0.878	0.871	0.869	0.878	0.869
L40-18-n	*	1800 1800	0.831	0.823	0.821	0.831	0.823	0.856	0.831	0.821
L40-21-n	*	2100 2100	0.842	0.832	0.830	0.842	0.832	0.871	0.842	0.830
L50-18-n	8.35	1800 1800	0.884	0.878	0.876	0.884	0.878	0.904	0.884	0.876
L50-21-n	8.35	2100 2100	0.839	0.832	0.830	0.839	0.832	0.895	0.839	0.830
L50-24-n	8.35	2400 2400	0.875	0.867	0.902	0.875	0.904	0.939	0.875	0.865
L40-15-w	6.68	1500 1500	0.945	0.938	0.936	0.945	0.938	0.936	0.945	0.936
L40-18-w	6.68	1800 1800	0.899	0.892	0.921	0.899	0.923	0.921	0.899	0.890
L40-21-w	*	2100 2100	0.870	0.862	0.895	0.870	0.898	0.931	0.870	0.860
L50-18-w	8.35	1800 1800	0.940	0.933	0.932	0.940	0.933	0.956	0.940	0.932
L50-21-w	8.35	2100 2100	0.845	0.839	0.865	0.845	0.867	0.921	0.874	0.837
L50-24-w	8.35	2400 2400	0.810	0.803	0.864	0.810	0.867	0.928	0.843	0.801

* no transition

Table 10. Weight comparison of sinusoidal web girders to flat web I-girders – 9mm minimum web thickness.

Designation	Transition Location (from end) (m)	Web Depth (mm)	Weight Ratio							
			Profile #1	Profile #2	Profile #3	Profile #4	Profile #5	Profile #6	Profile #7	Profile #8
L40-15-n	6.68	1500 1500	0.969	0.959	0.957	0.969	0.959	0.957	0.969	0.957
L40-18-n	*	1800 1800	0.940	0.928	0.925	0.940	0.928	0.925	0.940	0.925
L40-21-n	*	2100 2100	0.969	0.955	0.952	0.969	0.955	0.952	0.969	0.952
L50-18-n	8.35	1800 1800	0.972	0.962	0.960	0.972	0.962	0.960	0.972	0.960
L50-21-n	8.35	2100 2100	0.942	0.930	0.928	0.942	0.930	0.928	0.942	0.928
L50-24-n	8.35	2400 2400	0.992	0.979	0.976	0.992	0.979	0.976	0.992	0.976
L40-15-w	6.68	1500 1500	0.998	0.989	0.987	0.998	0.989	0.987	0.998	0.987
L40-18-w	6.68	1800 1800	0.995	0.984	0.982	0.995	0.984	0.982	0.995	0.982
L40-21-w	*	2100 2100	0.982	0.970	0.967	0.982	0.970	0.967	0.982	0.967
L50-18-w	8.35	1800 1800	0.990	0.982	0.979	0.990	0.982	0.979	0.990	0.979
L50-21-w	8.35	2100 2100	0.932	0.923	0.921	0.932	0.923	0.921	0.932	0.921
L50-24-w	8.35	2400 2400	0.910	0.899	0.896	0.910	0.899	0.928	0.910	0.896

* no transition

5.5. Observations from Preliminary Design Study

Corrugated web girders designed using shear and flexural strength information available at the beginning of the preliminary design study demonstrated the potential for weight savings when compared to conventional flat web I-girders. Based on shear strength considerations, the required thickness of the web was often less than the web thickness expected to be acceptable in practice. Assuming a minimum acceptable web thickness of 6mm (1/4in), the corrugated web girders demonstrated smaller, but still significant, potential for weight savings.

When sinusoidal webs were used instead of trapezoidal webs, the change in girder weight varied depending on the minimum web thickness assumed. When no limit on the web thickness was assumed, the difference in weight between a sinusoidal web girder and the corresponding trapezoidal web girder was between – 2% and +14%. When a 6mm (1/4in) minimum web thickness was assumed, the difference in weight was in the same range, however, the sinusoidal web girders were lighter in more cases. With a 9mm (11/32in) minimum web thickness, most cases showed an insignificant weight decrease (up to 3%) when sinusoidal corrugations were used.

Based on the shear strength criteria used in the study, local buckling did not appear to control the design in any case. Trapezoidal webs are more stable against global buckling than the corresponding sinusoidal webs. For the trapezoidal webs in the study, global buckling controlled the shear capacity of only the deep, thin webs with shallow corrugation depths. For most of the cases studied, the shear capacity of the trapezoidal webs was controlled by the shear yield strength and not by buckling. For sinusoidal webs, global buckling controlled the design of all the deep webs except for the ones with the largest corrugation depth.

Finally, the impacts of the corrugated web shear and flexural strength design criteria used in the preliminary design study should be considered. As noted at the beginning of Section 5, the work described in Sections 2, 3, and 4 of this report has produced more conservative recommendations for shear and flexural strength than those used in the preliminary design study

The recommended shear strength criteria limit the shear stress to 70.7% of the shear yield stress. The preliminary design study allowed up to 100% of the shear yield stress. Therefore, for the cases where no web thickness limit was assumed and the shear capacity was controlled by yield, the web would need to be approximately 41% thicker to satisfy the recommended design criteria. For the cases where no web thickness limit was assumed, the web weight is on average 21% of the girder weight, and therefore, a 41% increase in web thickness would increase the girder weight by 8%.

The recommended flexural strength criteria consider flange transverse bending of corrugated web girders under vertical shear force, however, the preliminary design study did not. If flange transverse bending were considered in the preliminary design study, it is estimated that the flange area, and therefore the flange weight, would increase by

approximately 3%. In addition, it should be noted, that the flange widths for the corrugated web girders were assumed to be the same as those of the flat web I-girders. If the flange widths were optimized for flange transverse bending, it is likely that this increase in flange weight would be reduced.

In conclusion, the preliminary design study demonstrated the potential for corrugated web girders to be lighter than conventional flat web girders by more than 20% when no web thickness limit is imposed, and by nearly 20% when the minimum web thickness is 6mm (1/4in). If the more conservative shear and flexural strength design criteria developed by other tasks in Work Area 1 had been used in the design study, this potential weight savings would decrease to roughly 11%. The design study shows no consistent weight savings advantage from using sinusoidal webs, rather than trapezoidal webs, and in some cases the sinusoidal webs result in heavier girders. For the range of span and girder spacing cases that were studied, the corrugated web girders with deeper webs were often the most efficient, and girder designs with deeper webs have greater potential to be economical.

6. Strength Design Criteria for Corrugated Web Girders

This section summarizes the recommended design criteria for corrugated web girders. The application of the criteria should be limited to girders with a corrugated web similar to that shown in Figure 5. The shear and flexural resistance criteria recommended here are intended to work within Section 6.10 of the AASHTO LRFD bridge design specifications (AASHTO 1998).

6.1. Design Criteria for Shear Resistance

The shear resistance criteria suggested here are to be used in place of Sections 6.10.7.2 and 6.10.7.3 of the AASHTO LRFD bridge design specifications to calculate V_n.

The global shear buckling capacity will reach the shear yield stress, τ_y , if the ratio of the web depth, h_w, to the web thickness, t_w, satisfies:

$$\frac{h_w}{t_w} \le 1.7\sqrt{\frac{E}{F_{yw}}\left(\frac{b}{t_w}\right)^{1.5} F(\alpha,\beta)} \tag{20}$$

where F(α,β) is the nondimensional coefficient characterizing the web corrugation geometry given by Equation 4. Equation 20 is derived from the formula for the global inelastic shear buckling stress, $(\tau_{cr,G})_{inel}$, given by Equation 5, with Equation 3 providing the elastic global shear buckling stress, $(\tau_{cr,G})_{el}$. The h_w / t_w limit of Equation 20 is taken as 90% of the largest h_w / t_w at which $(\tau_{cr,G})_{inel}$ from Equation 5 equals τ_y.

Provided that Equation 20 is satisfied, the nominal shear capacity, V_n, is calculated as follows from the local shear buckling stress:

If $\lambda_L \leq 2.586$, then:

$$V_n = 0.707\left(\frac{F_{yw}}{\sqrt{3}}\right)h_w t_w \tag{21}$$

If $2.586 < \lambda_L \leq 3.233$, then:

$$V_n = \sqrt{\frac{1}{1+0.150\lambda_L^2}}\left(\frac{F_{yw}}{\sqrt{3}}\right)h_w t_w \tag{22}$$

If $\lambda_L \geq 3.233$, then:

$$V_n = \sqrt{\frac{1}{1+0.0143\lambda_L^4}}\left(\frac{F_{yw}}{\sqrt{3}}\right)h_w t_w \tag{23}$$

where, λ_L expresses the local buckling slenderness in a normalized form and is given by:

$$\lambda_L = \frac{w}{t_w}\sqrt{\frac{F_{yw}}{E}} \tag{24}$$

Equations 21, 22, and 23 are derived from Equations 1, 5, and 6 as follows. First, the value of λ_L when $(\tau_{cr,L})_{inel} = \tau_y$ is calculated from Equation 5. The result is λ_L =2.586. Then, the value of λ_L when Equation 1 equals Equation 5 is calculated as λ_L =3.233. The shear capacity of Equation 21 is determined from Equation 7 when the inelastic local buckling capacity (from Equation 5) equals τ_y and the global buckling capacity (from Equation 5) equals τ_y (because Equation 20 is satisfied). The value of τ_y is determined from Equation 6. The shear capacity of Equation 22 is determined from Equation 7 when the inelastic local buckling capacity (from Equation 5) is less than τ_y and the global buckling capacity (from Equation 5) equals τ_y. The shear capacity of Equation 23 is determined from Equation 7 when the elastic local buckling capacity is calculated from Equation 1 and the global buckling capacity equals τ_y.

6.2. Design Criteria for Flexural Resistance

The flexural resistance criteria suggested here are intended to work within Section 6.10.4 of the AASHTO LRFD bridge design specifications.

Flange Stresses. Two types of stresses develop in the flanges of corrugated web I-girders:

1. Flange stresses due to overall girder (primary) bending are calculated with the web contribution to bending strength neglected. These flange stresses are assumed uniformly distributed across the flange width. In regions of zero vertical shear force (*i.e.*, constant moment regions), these primary bending stresses are the only calculated flange stresses.

2. In regions of nonzero vertical shear force, flange transverse bending moments (*i.e.*, bending moments about a vertical axis) develop as discussed in Section 4.2. The distribution and magnitude of these transverse moments, M_t, will vary along the length of the flanges. Based on Equation 19, a simple formula to calculate the first order design transverse bending moment for the flanges of a girder with trapezoidal corrugations, $(M_{t1})_{des}$ is:

$$\left(M_{t1}\right)_{des} = \frac{V^{ref}}{h_w}\left(b + \frac{d}{2}\right)h_r \tag{25}$$

where V^{ref} is a reference vertical shear force used to calculate the flange transverse bending, and b, d, and h_r are corrugated web geometry parameters shown in Figure 1.

Equation 25 is applicable when: (1) each girder reaction is located at the center of an inclined fold and, thus, the girder span is n times the corrugation wave length with n being a whole number multiple of 1/2 (*i.e.*, 1/2, 2/2, 3/2, *etc*.), and (2) at least one interior cross-frame is provided within the span.

As discussed below, $(M_{t1})_{des}$ should be combined with the overall girder bending moment in the design of the flanges. In most situations, the shear, V^{ref}, used to calculate $(M_{t1})_{des}$ at a given cross section should be the value of the factored vertical shear force envelope at that cross section. However, in some situations, the shear force envelope values near cross sections of maximum overall girder bending moment may be small, resulting in an unconservative estimate of $(M_{t1})_{des}$. Thus, V^{ref} should not be less than 25% of the maximum factored shear force in the span.

For the design of compression flanges, the moment from Equation 25, $(M_{t1})_{des}$, which is a first order bending moment, should be amplified as follows:

$$\left(M_t\right)_{des} = \frac{\left(M_{t1}\right)_{des}}{1 - \dfrac{M_u}{S_{xc} \cdot F_{cr}}} \tag{26}$$

where, $(M_t)_{des}$ is the amplified flange transverse bending moment for the compression flange, M_u is the factored overall girder bending moment, S_{xc} is the section modulus to the compression flange for overall girder bending (calculated with the web contribution neglected), and F_{cr} is the elastic lateral-torsional buckling stress calculated as follows:

$$F_{cr} = \frac{9.86E}{\left(\frac{L_b}{r_t}\right)^2} \tag{27}$$

where

$$r_t = \frac{b_{fc}}{\sqrt{12}} \tag{28}$$

and b_{fc} is the width of the compression flange and L_b is the unbraced length. For the design of tension flanges, the amplification factor is not needed, and $(M_t)_{des} = (M_{t1})_{des}$.

Flexural Strength Limit State for Compact Sections. To account for transverse bending of the flanges when vertical shear forces act on a corrugated web girder with compact flanges, the suggested approach is similar to the approach of the AASHTO LRFD specifications for wind effects on a conventional flat web I-girder. The transverse moment is assumed to be carried by a width, b_w, at each edge of the flange:

$$b_w = \frac{b_f - \sqrt{b_f^2 - \frac{4(M_t)_{tot}}{t_f F_{yf}}}}{2} \le \frac{b_f}{2} \tag{29}$$

where $(M_t)_{tot}$ is the total factored transverse bending moment acting on the flange, b_f is the flange width and t_f is the flange thickness. Equation 29 is similar to Equation (6.10.3.5.1-1) of the AASHTO LRFD specifications, however, Equation 29 should be applied to both the top and bottom flanges for a non-composite section.

For the top flange of a non-composite section, $(M_t)_{tot} = (M_t)_{des}$. When the steel section is composite with the concrete deck, the effect of the transverse moment on the top flange is neglected (*i.e.*, $(M_t)_{tot} = 0$ and $b_w = 0$) for conditions after the concrete deck hardens. For the bottom flange, $(M_t)_{tot} = (M_t)_{des}$ for load combinations without wind load, and $(M_t)_{tot} = (M_t)_{des} + M_w$ for load combinations with wind load, where M_w is the flange transverse moment due to the wind load.

For a compact section, the required resistance calculations are made for an effective section obtained by removing the width, b_w, from each side of the flanges. For a composite section, b_w is removed from the bottom flange only (since $b_w = 0$ for the top flange). For a non-composite section, b_w is removed from both flanges.

For the nominal flexural strength of compact sections, M_n, a simplified calculation is recommended which provides flexural strength similar to, but less than, the plastic

moment, M_p. Three assumptions of this calculation are: (1) the corrugated web does not contribute to the flexural resistance of a corrugated web girder; (2) the top flange in a composite section in positive flexure does not contribute significantly to the ultimate flexural strength, and (3) the steel reinforcement in the concrete deck of a composite section in negative flexure does not contribute significantly to the ultimate flexural strength. Assumption (1) was discussed earlier. Assumptions (2) and (3) are conservative and simplify the calculation.

For composite sections in positive flexure, M_n is calculated as follows:

If $0.85 f_c' b_{slab} t_{slab} \geq F_{yf}(b_{bf} - 2b_{bw})t_{bf}$

$$M_n = F_{yf}(b_{bf} - 2b_{bw})t_{bf}(h_w + t_{tf} + t_{slab} + 0.5t_{bf} - 0.5a) \tag{30}$$

where, $a = (F_{yf}(b_{bf} - 2b_{tw})t_{bf})/(0.85 f_c' b_{slab})$.

Otherwise

$$M_n = 0.85 f_c' b_{slab} t_{slab}(h_w + t_{tf} + 0.5(t_{slab} + t_{bf})) \tag{31}$$

In the above equations, b_{slab} is the effective width of the slab, t_{slab} is the thickness of the slab, f_c' is the specified compressive strength of the slab concrete, F_{yf} is the specified flange yield stress, the subscript "*b*" refers to the bottom flange, the subscript "*t*" refers to the top flange, and the subscript "*w*" refers to flange widths calculated using Equation 29.

For non-composite sections in positive flexure as well as both composite and non-composite sections in negative flexure, M_n is calculated as follows:

If $F_{yf}(b_{tf} - 2b_{tw})t_{tf} \geq F_{yf}(b_{bf} - 2b_{bw})t_{bf}$

$$M_n = F_{yf}(b_{bf} - 2b_{bw})t_{bf}(h_w + (t_{tf} + t_{bf})/2) \tag{32}$$

Otherwise

$$M_n = F_{yf}(b_{tf} - 2b_{tw})t_{tf}(h_w + (t_{tf} + t_{bf})/2) \tag{33}$$

For the strength limit state, the flexural strength is satisfactory when $M_r = \varphi_f M_n$ equals or exceeds the factored overall girder bending moment, M_u.

Compact section criteria for a corrugated web girder may be taken as follows:

$$\lambda_f = \frac{b_f + (h_r/2)}{2t_f} \leq 0.382\sqrt{\frac{E}{F_{yf}}} \tag{34}$$

$$L_b \le (0.124 - 0.0759(M_l/M_n))\frac{r_y E}{F_{yf}} \tag{35}$$

where, F_{yf} is the specified yield stress of the compression flange, M_l is the lower moment due to the factored loading at either end of the unbraced length, L_b, and r_y is the radius of gyration of the steel section, with respect to the vertical axis (calculated including the web area, $h_w t_w$, but neglecting the web corrugations).

Equation 34 is similar to Equation (6.10.4.1.3-1) of the AASHTO LRFD specifications except that $(b_f+(h_r/2))/2$ is used as the flange overhang instead of $b_f/2$ as discussed in Section 4.1. Equation 35 is identical to Equation (6.10.4.1.7-1) of the AASHTO LRFD specifications. Equations 34 and 35 are applicable to non-composite sections in both positive and negative flexure, and to composite sections in negative flexure. Composite sections in positive flexure should be treated as compact sections.

Because the web does not carry any significant bending moment and therefore does not suffer from bend buckling, there are no flexure-based web slenderness criteria, and only Equations 34 and 35 are necessary to check for section compactness.

Flexural Strength Limit State for Non-Compact Sections. To account for flange transverse bending of corrugated web girders under the action of vertical shear forces, the recommended approach is similar to the approach of the AASHTO LRFD specifications for wind effects on girder flanges with non-compact sections. The flange stresses are calculated by superposing stresses due to overall girder (primary) bending and flange transverse (secondary) bending as follows:

$$f_f = \left|\frac{M_u}{S_x}\right| + \left|\frac{6(M_t)_{tot}}{t_f b_f^2}\right| \tag{36}$$

where, M_u is the factored overall (primary) bending moment, $(M_t)_{tot}$ is the total factored transverse bending moment acting on the flange, and S_x (calculated with the web contribution neglected), b_f, and t_f are the section modulus, width, and thickness for the appropriate flange. Equation 36 is similar in concept to Equations (6.10.3.5.2-1) and (6.10.3.5.2-2) of the AASHTO LRFD specifications, however, Equation 36 should be applied to both top and bottom flanges for a non-composite section.

For the top flange of a non-composite section, $(M_t)_{tot} = (M_t)_{des}$. For the top flange of a composite section, the effect of the transverse moment is neglected (*i.e.*, $(M_t)_{tot} = 0$) for conditions after the concrete deck hardens. For the bottom flange, $(M_t)_{tot} = (M_t)_{des}$ for load combinations without wind load, and $(M_t)_{tot} = (M_t)_{des} + M_w$ for load combinations with wind load.

Similar to Equation (6.10.3.5.2-1) of the AASHTO LRFD specifications, the flange stresses f_f calculated from Equation 36, should be less than or equal to the factored nominal flexural resistance of the flange, $F_r = \varphi_f F_n$. That is, $f_f \leq \varphi_f F_n$. Criteria for calculating F_n are as follows.

For tension flanges, $F_n = F_{yf}$. For the compression flanges of non-composite sections in positive or negative flexure, and the compression flanges of composite sections in negative flexure:

$$F_n = min\left(F_{fb}, F_{lt}\right) \tag{37}$$

F_{fb} is the flange local buckling resistance:

$$F_{fb} = F_{yf}\left[1.0 - 0.88\left(\lambda_f \sqrt{\frac{F_{yc}}{E}} - 0.38\right)\right] \leq F_{yf} \tag{38}$$

where λ_f is given by Equation 34. λ_f *should be less than 14.5*.

F_{lt} is the lateral torsional buckling resistance given by the following equations:

If $L_b \leq L_r$, then:

$$F_{lt} = C_b \cdot F_{yf}\left[1.33 - 0.187\left(\frac{L_b}{r_t}\right)\sqrt{\frac{F_{yc}}{E}}\right] \leq F_{yf} \tag{39}$$

Otherwise:

$$F_{lt} = C_b \cdot \left[\frac{9.86E}{\left(\frac{L_b}{r_t}\right)^2}\right] \leq F_{yf} \tag{40}$$

where

$$L_r = 4.44 r_t \sqrt{\frac{E}{F_{yf}}} \tag{41}$$

and C_b is the moment gradient factor from Equation (6.10.4.2.5a-4) of the AASHTO LRFD specifications. Note that Equation 38 is an inelastic flange local buckling resistance equation that will replace the local buckling resistance (Equation (6.10.4.2.4a-2)) of the current AASHTO LRFD specifications, and Equations 39 and 40 are similar to Equations (6.10.4.2.5a-1) and (6.10.4.2.5a-2) of the current AASHTO LRFD specifications.

Also, note that the hybrid factor, R_h, and the load shedding factor, R_b, in AASHTO LRFD Equations (6.10.4.2.5a-1) and (6.10.4.2.5a-2) are taken equal to one because a web contribution is not included in the flexural strength calculations.

Service Limit State for Control of Permanent Deflections. The calculations of elastic stresses for this limit state are similar to the calculations for a conventional I-girder as given in Section 6.10.5.2.of the AASHTO LRFD specifications.

For composite sections, the sum of the overall girder bending stresses, similar to that calculated for a conventional flat web I-girder, is calculated from three conditions: (1) appropriate factored component dead loads acting on the steel section alone, (2) appropriate factored superimposed dead loads acting on the long-term composite section, and (3) appropriate factored live loads acting on the short-term composite section.

For the bottom flange, the total flange stress, f_f, is calculated by adding the following transverse bending stress, f_t to the absolute value of the sum of the overall girder bending stresses:

$$f_t = \left| \frac{6(M_t)_{des}}{t_f b_f^2} \right| \tag{26}$$

For the top flange, f_t, is neglected, and f_f is equal to the sum of the overall girder bending stresses.

For both flanges, the total flange stress, f_f, should be less than or equal to 95% of the flange yield stress, that is, $f_f \leq 0.95F_{yf}$.

For non-composite sections, the sum of the overall girder bending stresses is similar to that for a conventional flat web I-girder and is calculated from the all of the appropriate factored dead loads and live loads acting on the steel section alone. For the top and bottom flanges, the total flange stress, f_f, is calculated by adding f_t from Equation (26) to the absolute value of the sum of the overall girder bending stresses.

For both flanges, the total flange stress, f_f, should be less than or equal to 80% of the flange yield stress, that is, $f_f \leq 0.80F_{yf}$.

7. Recommended Corrugation Geometry

The corrugation geometry recommended for the demonstration bridge is shown in Figure 5. The recommendation is based on the results of Work Area 1, as presented in this report, as well as the results of Work Area 2 (Sause 2003) and Work Area 3 (Sause *et al*. 2003). The selection of the corrugation geometry involves two major decisions: (1) selection of the web shape (*i.e.*, sinusoidal or trapezoidal); and (2) selection of the corrugation wave parameters (*e.g.*, wave length, corrugation depth, *etc.*).

Only sinusoidal and trapezoidal shapes were considered. Other shapes are possible, but information in the literature on structural behavior, fabrication, and so on, was limited to sinusoidal and trapezoidal shapes. The studies undertaken in Work Area 1 found that

more information existed on trapezoidal web girders (*e.g.*, Elgaaly *et al.* 1996; Elgaaly *et al.* 1997; Elgaaly and Seshadri 1998; Johnson and Cafolla 1997; Lindner and Aschinger 1988; Lindner and Aschinger 1990; Lindner 1990; and Lindner and Huang 1995) than on sinusoidal web girders. As a result, the existing shear and flexural strength information from the literature could be used in the preliminary design study of trapezoidal web girders (Section 5). A similar body of information did not exist for sinusoidal web girders, and the preliminary design study of sinusoidal web girders had to extrapolate from the existing information on trapezoidal web girders. This existing information also enabled trapezoidal web test specimens to be designed for tests conducted in Work Area 1 and Work Area 3. The results of the preliminary design study did not demonstrate any significant advantages for sinusoidal web girders. In addition, the corrugated web girder fabrication studies in Work Area 2 (Sause 2003) found that trapezoidal web girders were easier to fabricate. Therefore the trapezoidal shape was selected for the demonstration bridge.

The corrugation parameters to be determined for a trapezoidal web are shown in Figure 1. A study of available corrugation geometries (Figure 26) showed that (except for Profile #8 which was designed for the demonstration bridge) existing corrugation geometries had relatively small values for b, d, and h_r because these geometries were intended for relatively thin web plate. For the demonstration bridge, a minimum web thickness, t_w, of 6mm (1/4in) was selected. As a result, the fold dimensions b and c could be increased to values greater than those of the existing corrugation geometries, without concern for a decrease in local buckling resistance. A longitudinal fold width b = 300mm (11.8in) was selected for the demonstration bridge, and Figure 3 shows that the fold slenderness ratio, based on this selected longitudinal fold width (*i.e.*, $w = b$), is within the range where the local buckling strength is maximum.

The selected corrugation angle, α , was based on the suggestion of Lindner and Huang (1995), that α should not be less than 30° so that the longitudinal and inclined folds provide sufficient support for one another at the fold lines to mobilize the full shear capacity of each fold. The selected angle, α = 36.9°, provides simple ratios of 3 to 4 for h_r to d, and 3 to 5 for h_r to c (see Figures 1 and 5). The corrugation depth, h_r, was selected to provide a margin against global buckling that permits the corrugation geometry to be used with relatively deep webs. For example, with h_r = 150mm (5.9in) and a web thickness t_w = 6mm (1/4in), the web depth, h_w, must exceed 3050mm (10ft), before the global buckling limit of Equation 20 is violated. For a larger value of t_w, an even larger web depth, h_w, could be used. Therefore, the selected h_r allows the selected corrugation geometry to be used over a wide range of web depths. With h_r = 150mm (5.9in), the remaining parameters are c = 250mm (9.8in) and d = 200mm (7.9in). The resulting combination of b and d provides a convenient corrugation wave length of 1000mm (1m or 39.4in). With minor modifications, the corrugation geometry can be adjusted to convenient dimensions in customary U.S. units of b = 12in, h_r = 6in, c = 10in, and d = 8in, with a wave length of 40in. Finally, the selected corrugation geometry has a bend radius at the fold lines r = 120mm (4.7in), which gives an r/t_w ratio of 20. As discussed in Sause *et al.* (2003), this relatively large bend radius maintains good fracture toughness characteristics in the bend region and enhances the fatigue life.

8. Summary and Conclusions

This report presents Work Area 1 of the Pennsylvania High Performance Steel (HPS) Bridge Demonstration Project. The report establishes design criteria for the shear and flexural strength of corrugated web girders, and recommends a corrugation shape for the girders of the demonstration bridge. The design criteria (Section 6) are presented in a form that is compatible with the AASHTO LRFD bridge design specifications (AASHTO 1998). The recommended corrugation shape (Section 7) should have applicability over a wide range of girder spans, spacings, and web depths.

In addition, the report summarizes previous shear strength theory and test results for corrugated web girders (Section 2), and presents new shear strength criteria (Section 3). The large-scale shear strength tests of HPS-485W (HPS-70W) steel corrugated web girders that were conducted as part of Work Area 1 are presented (Section 4). Previous flexural strength theory and test results are summarized and new flexural theory is presented. A preliminary design study of corrugated web girders is presented (Section 5).

From the study of existing shear strength theory and test results it was concluded that the theory (Equations 1 and 5) could not be used to estimate the nominal shear strength of bridge girders with corrugated webs. A clear reason for the discrepancy between the theory and test results was not determined, but out-of-flatness of the folds of corrugated webs may be an important factor. An alternative formula for the nominal shear strength is proposed (Equation 7). The large-scale shear strength tests of two of HPS-485W (HPS-70W) corrugated web girders showed that the proposed shear strength formula is conservative for girders with the corrugation shape selected for the demonstration bridge.

Based on the study of previous flexural strength theory and test results, and from new research performed by Abbas (2003), new flexural strength theory was developed to consider the flange transverse bending that occurs when corrugated web girders carry vertical shear forces. The transverse bending moment should be considered in the design of corrugated web girders, and the report summarizes two methods of analysis. The flexural strength design criteria recommended in Section 6 include the effects of flange transverse bending.

The preliminary design study, based on information available at the beginning of the project, demonstrated the potential for corrugated web girders to be lighter than conventional flat web girders by more than 20% when no web thickness limit is imposed, and by nearly 20% when the minimum web thickness is 6mm (1/4in). If the more conservative shear and flexural strength design criteria developed in Work Area 1 had been used in the design study, this potential weight savings would decrease to roughly 11%. The design study shows no consistent weight savings advantage from using sinusoidal webs, rather than trapezoidal webs. The corrugated web girders with deeper webs were often more efficient than those with shallower webs, and corrugated web girders with deeper webs have greater potential to be economical.

References

AASHTO (1998) *AASHTO LRFD Bridge Design Specifications*, 2nd edition, American Association of State Highway and Transportation Officials, Washington, D.C.

Abbas, H.H. (2003) "Analysis and Design of Corrugated Web I-Girders for Bridges Using High Performance Steel, " Ph.D. Dissertation, Lehigh University, Bethlehem, PA.

ASTM (2001) "A709/A709M-00a, Standard Specification for Carbon and High-Strength Low-Alloy Structural Steel Shapes, Plates, and Bars and Quenched-and-Tempered Alloy Structural Steel Plates for Bridges," *ASTM Annual Book of Standards, Vol. 01.04*, American Society for Testing and Materials, West Conshohocken, PA.

Easley, J.T. (1975) "Buckling Formulas for Corrugated Metal Shear Diaphragms," *ASCE Journal of the Structural Division*, Vol. 101, No. ST7 (July), pp. 1403-1417.

Elgaaly, M., Hamilton, R.W., and Seshadri, A. (1996) "Shear Strength of Beams with Corrugated Webs," *ASCE Journal of Structural Engineering*, Vol. 122, No. 4 (April), pp. 390-398.

Elgaaly, M., Seshadri, A., and Hamilton, R.W. (1997) "Bending Strength of Steel Beams with Corrugated Webs," *ASCE Journal of Structural Engineering*, Vol. 123, No. 6 (June), pp. 772-782.

Elgaaly M. and Seshadri A. (1998) "Steel Built-up Girders with Trapezoidally Corrugated Webs," *AISC Engineering Journal*, First Quarter, pp. 1-11.

Hibbitt, Karlsson, and Sorenson, Inc. (1998) *ABAQUS Version 5.8*, Hibbitt, Karlsson, and Sorenson, Inc., Pawtucket, RI.

Johnson, R.P. and Cafolla, J. (1997) "Local Flange Buckling in Plate Girders with Corrugated Webs," *Proceedings, Instn Civ Engrs Structs & Bldgs*, Vol. 123, May, pp. 148-156.

Lindner, J. and Aschinger, R. (1988) "Grenzschubtragfähigkeit von I-trägern mit Trapezförmig Profilierten Stegen," *Stahlbau*, Vol. 57, No. 12, pp. 377-380, 1988.

Lindner, J. and Aschinger, R. (1990) "Zur Torsionssteifigkeit von Trapezstegträgern," *Stahlbau*, Vol. 59, No. 4, pp. 113-120.

Lindner, J. and Huang, B. (1995) "Beulwerte für Trapezförmig Profilierte Bleche unter Schubbeanspruchung," *Stahlbau*, Vol. 64, No. 12, pp. 370-374.

Lindner, J. (1990) "Lateral Torsional Buckling of Beams with Trapezoidally Corrugated Webs," *Proceedings, Intl. Colloquium of Stability of Steel Structures*, Budapest, pp. 79-86.

Peil, U. (1998) "Statische Versuche an Trapezstegträgern Untersuchung der Querkraftbeanspruchbarkeit," Report, Institut für Stahlbau, Technische Universität Braunschweig, Braunschweig.

Sause, R., Abbas, H.H., Driver, R.G., Anami, K., and Fisher, J.W. (2003) "Fatigue Resistance of Corrugated Web Girders: Work Area 3, Pennsylvania Innovative High Performance Steel Bridge Demonstration Project," ATLSS Report No. 03-20, Center for Advanced Technology for Large Structural Systems, Lehigh University, Bethlehem, PA, September.

Sause, R. (2003) "Corrugated Web Girder Fabrication: Work Area 2, Pennsylvania Innovative High Performance Steel Bridge Demonstration Project," ATLSS Report No. 03-19, Center for Advanced Technology for Large Structural Systems, Lehigh University, Bethlehem, PA, August.

Timoshenko, S.P. and Gere, J.M (1961) *Theory of Elastic Stability*, 2nd Edition, McGraw-Hill Book Company, Inc.